Mid-latitude mixed-phase stratocumulus clouds and their interactions with aerosols: how ice processes affect microphysical, dynamic and thermodynamic development in those clouds and interactions?

Seoung Soo Lee[1,2], Kyung-Ja Ha[2,3,4], M. G. Manoj[5], Mohammad Kamruzzaman[6,7]

Hyungjun Kim[8], Nobuyuki Utsumi[9], Youtong Zheng[10], Chang-Hoon Jung[11], Junshik Um[12]

Jianping Guo[13], Kyoung Ock Choi[14,15], Go-Un Kim[16]

[1]Earth System Science Interdisciplinary Center, University of Maryland, College Park, Maryland, USA

[2]Research Center for Climate Sciences, Pusan National University, Busan, Republic of Korea

[3]Center for Climate Physics, Institute for Basic Science and BK21 School of Earth and Environmental Systems, Pusan National University, Busan, Republic of Korea

[4]Center for Climate Physics, Institute for Basic Science, Busan, Republic of Korea

[5]Advanced Centre for Atmospheric Radar Research, Cochin University of Science and Technology, Kerala, India

[6]School of Mathematical Sciences, University of Adelaide, Adelaide, Australia

[7]Natural and Built Environments Research Centre, Division of Information Technology, Engineering and the Environment (ITEE), University of South Australia, Adelaide, Australia

[8]Institute of Industrial Science, University of Tokyo, Tokyo, Japan

[9]Nagomori Institute of Actuators, Kyoto University of Advanced Science, Japan

43 [10]The Program in Atmospheric and Oceanic Sciences, Princeton University, Princeton,

44 New Jersey, USA

45 [11]Department of Health Management, Kyungin Women's University, Incheon, Republic of

46 Korea

47 [12]Department of Atmospheric Sciences, Division of Earth Environmental System, Busan,

48 Republic of Korea

49 [13]State Key Laboratory of Severe Weather, Chinese Academy of Meteorological

50 Sciences, Beijing 100081, China

51 [14]Department of Atmospheric Sciences, University of Washington, Seattle, Washington,

52 USA

53 [15]Department of Atmospheric Sciences, Yonsei University, Seoul, Republic of Korea

54 [16]Marine Disaster Research Center, Korea Institute of Ocean Science and Technology,

55 Pusan, Republic of Korea

57
58

65 Corresponding author: Seoung Soo Lee

66 Office: (303) 497-6615

67 Cell: (609) 375-6685

68 Fax: (303) 497-5318

69 E-mail: cumulss@gmail.com, slee1247@umd.edu

Abstract

Mid-latitude mixed-phase stratocumulus clouds and their interactions with aerosols remain poorly understood. This study examines the roles of ice processes in those clouds and their interactions with aerosols using a large-eddy simulation (LES) framework. Cloud mass becomes much lower in the presence of ice processes and the Wegener-Bergeron-Findeisen (WBF) mechanism in the mixed-phase clouds as compared to that in warm clouds. This is because while the WBF mechanism enhances the evaporation of droplets, the low concentration of aerosols acting as ice nucleating particles (INP) and cloud ice number concentration (CINC) prevent the efficient deposition of water vapor. Note that the INP concentration in this study is based on the observed spatiotemporal variability of aerosols. This results in the lower CINC as compared to that with empirical dependence of the INP concentrations on temperature in a previous study. In the mixed-phase clouds, the increasing concentration of aerosols that act as cloud condensation nuclei (CCN) decreases cloud mass by increasing the evaporation of droplets through the WBF mechanism and decreasing the intensity of updrafts. In contrast to this, in the warm clouds, the absence of the WBF mechanism makes the increase in the evaporation of droplets inefficient, eventually enabling cloud mass to increase with the increasing concentration of aerosols acting as CCN. Here, the results show that when there is an increasing concentration of aerosols that act as INP, the deposition of water vapor is more efficient than when there is the increasing concentration of aerosols acting as CCN, which in turn enables cloud mass to increase in the mixed-phase clouds.

Deleted: ¶
¶
¶

1. Introduction

Stratiform clouds such as the stratus and stratocumulus clouds play an important role in global hydrologic and energy circulations (Warren et al. 1986, 1988; Stephens and Greenwald 1991; Hartmann et al. 1992; Hahn and Warren 2007; Wood, 2012). Aerosol concentrations have increased significantly as a result of industrialization. Increasing aerosols are known to decrease droplet size and thus increase the albedo of stratiform clouds (Twomey, 1974, 1977). Increasing aerosols may also suppress precipitation and, hence, alter the mass and lifetime of those clouds (Albrecht, 1989; Guo et al., 2016). These aerosol effects strongly depend on how increasing aerosols affect entrainment at the tops of the planetary boundary layer (PBL) (Ackerman et al., 2004) and disrupt global hydrologic and energy circulations. However, these effects are highly uncertain and thus act to cause the highest uncertainty in the prediction of future climate (Ramaswamy et al., 2001; Forster et al., 2007). Most of the previous studies on stratiform clouds and their interactions with aerosols to reduce the uncertainty have dealt with warm stratiform clouds and have seldom considered ice-phase cloud particles (e.g., ice crystals) (Ramaswamy et al., 2001; Forster et al., 2007; Wood, 2012). In reality, especially during wintertime when the surface temperature approaches the freezing temperature, stratiform clouds frequently involve ice particles and associated processes such as deposition and freezing. Since particularly in midlatitudes, stratiform clouds are generally way below the altitude of homogeneous freezing, in these clouds, liquid and ice particles usually co-exist.

The water-vapor equilibrium saturation (or saturation pressure) is lower for ice particles than for liquid particles. In mixed-phase clouds where liquid- and ice-phase hydrometeors coexist, when a given water-vapor pressure is higher than the equilibrium pressure for liquid particles, ice and liquid particles grow together via deposition and condensation, respectively, while competing for water vapor. When a given water-vapor pressure is lower than or equal to the equilibrium pressure for liquid particles, ice (liquid) particles can experience supersaturation (undersaturation or saturation). In this situation, liquid particles evaporate, while water vapor is deposited onto ice crystals. Water vapor in the air, which is depleted by the deposition onto ice crystals, is re-supplied by water vapor that is produced by the evaporation of droplets. The re-supplied water vapor in turn deposits onto

151 ice crystals. In other words, due to differences in the water-vapor equilibrium saturation
152 pressure between ice and liquid particles, ice particles eventually grow at the expense of
153 liquid particles. This is so-called Wegener-Bergeron-Findeisen (WBF) mechanism
154 (Wegener 1911; Bergeron 1935; Findeisen 1938).

155   The occurrence of the WBF mechanism depends on updrafts, humidity, associated
156 supersaturation and microphysical factors such as cloud-particle concentrations and sizes
157 (Korolev, 2007). Also, it needs to be pointed out that when the WBF mechanism starts and
158 how long it lasts depend on how a timescale for updrafts and associated supersaturation is
159 compared to that for phase-transition processes as a part of microphysical processes
160 (Pruppacher and Klett, 1978). Korolev (2007) have utilized a parcel-model concept to
161 come up with conditions of updrafts and microphysical factors where the WBF mechanism
162 is operative.

163   The evolution of cloud particles as well as their interactions with aerosols is strongly
164 dependent on thermodynamic and dynamic conditions such as humidity, temperature and
165 updraft intensity (Pruppacher and Klett, 1978; Khain et al., 2008). Interactions between ice
166 and liquid particles in mixed-phase clouds, which include the WBF mechanism, change
167 thermodynamic and dynamic conditions where cloud particles grow. Impacts of these
168 changes on the development of mixed-phase clouds and their interactions with aerosols
169 have not been understood well.

170   Over the last decades, numerous studies have been performed to improve our
171 understanding of mixed-phase clouds by focusing on clouds in the Arctic and over the
172 Southern Ocean. It has been found that the prevalence of mixed-phase clouds over the
173 Arctic enables them to have a substantial impact on radiative and hydrologic circulations
174 (e.g., Shupe et al., 2001, 2005; Intrieri et al., 2002; Dong and Mace, 2003; Zuidema et al.,
175 2005; Hu et al., 2010; Kanitz et al., 2011; Morrison et al., 2011; Huang et al., 2012). In
176 addition, Rangno and Hobbs (2001), Lohmann (2002) and Borys et al. (2003) have
177 proposed not only cloud condensation nuclei (CCN) but also ice nucleating particles (INP)
178 affect mixed-phase clouds by altering microphysical variables (e.g., number concentrations
179 and sizes of cloud particles) and dynamic variables (e.g., updrafts). However, Lance et al.
180 (2010) and Jackson et al. (2012) have indicated that these aerosol effects on mixed-phase
181 clouds have not been clearly identified due to lack of data of meteorological and cloud

182   conditions in which aerosols influence those clouds. Naud et al. (2014) and Bodas-Salcedo

183   et al. (2016) have reported that climate models have not been able to represent mixed-

184   phased clouds and their interactions with aerosols reasonably well and this has been one

185   important reason why climate models have produced large errors in simulating energy and

186   hydrologic budgets and circulations. Young et al. (2017) have reported that the

187   parametrization of ice-crystal nucleation can be a key reason for the misrepresentation of

188   mixed-phase clouds in models.

189   This study aims to gain a better understanding of mixed-phase stratocumulus clouds

190   and interactions between those clouds and aerosols. The better understanding enables us to

191   gain a more general understanding of stratiform clouds and their interactions with aerosols,

192   which better elucidates roles of clouds and aerosol-cloud interactions in climate. This in

193   turn provides valuable information to better parameterize stratiform clouds and interactions

194   for climate models. To fulfill the aim, this study focuses on effects of the interplay between

195   ice crystals and droplets on those clouds, and interactions of these effects with aerosols

196   using a large-eddy simulation (LES) Eulerian framework. The LES framework reasonably

197   resolves microphysical and dynamic processes at turbulence scales and thus we can obtain

198   process-level understanding of those effects and interactions. Note that with the Eulerian

199   framework, instead of tracking down individual air parcels, which can be pursued with the

200   Lagrangian framework, this study looks at updrafts, microphysical factors, phase-transition

201   processes and their evolution, which are averaged over grid points in a domain, to examine

202   the overall interplay between ice and liquid particles over the whole domain. Also, in the

203   LES framework, air parcels go through various updrafts, microphysical factors and

204   feedbacks between them. Thus, unlike in Korolev (2007), an air parcel in the LES

205   framework can repeatedly experience conditions where the WBF mechanism does not

206   work and those where the mechanism works as it moves around three-dimensionally.

207   Hence, chasing down air parcels in terms of conditions (e.g., updrafts and microphysical

208   factors) for processes such as the WBF mechanism is enormous task and not that viable.

209   This motivates us to embrace the approach that adopts the averaged updrafts, microphysical

210   factors and phase-transition processes to examine the overall interplay between ice and

211   liquid particles which includes the WBF mechanism. To help this approach to identify the

212 overall interplay between ice and liquid particles clearly, this study utilizes sensitivity
213 simulations.
214   Mixed-phase stratiform clouds have been formed frequently over the Korean
215 Peninsula in midlatitudes. These clouds have been affected by the advection of aerosols
216 from East Asia (e.g., Lee et al., 2013; Oh et al., 2015; Eun et al., 2016; Ha et al., 2019).
217 However, we do not have a clear understanding of those clouds and impacts of those
218 aerosols, which are particularly associated with the industrialization of East Asia, on them
219 in the Peninsula (Eun et al., 2016). Motivated by this, we examine those clouds and effects
220 of the advected aerosols from East Asia on them over an area in the Korean Peninsula as a
221 way of better understanding those clouds and aerosol-cloud interactions in them.
222
223   **2. Case description**
224
225 A system of mixed-phase stratocumulus clouds was observed in the Seoul area in Korea
226 over a period between 00:00 LST (local solar time) on January 12th and 00:00 LST on
227 January 14th in 2013. The Seoul area is a conurbation area composed of the Seoul capital
228 city and adjacent highly populated cities. The population of the Seoul area is estimated at
229 twenty-five million. Coincidently, during this period, there is advection of an aerosol layer
230 from the west of the Seoul area (or from East Asia) to it and this lifts aerosol concentrations
231 in the Seoul area. This type of advection has been monitored by island stations in the
232 Yellow Sea (Eun et al., 2016; Ha et al., 2019). For this study, the advection is monitored
233 and identified by comparisons in PM_{10} and $PM_{2.5}$, representing aerosol mass, between a
234 ground station in Baekryongdo island, located in the Yellow Sea, and ground stations in
235 and around the Seoul area. These stations observe and measure PM10 and PM2.5 using the
236 beta-ray attenuation method (Eun et al., 2016; Ha et al., 2019). PM stands for particulate
237 matter and PM_{10} ($PM_{2.5}$) is the total mass of aerosol particles whose diameter is smaller
238 than 10 (2.5) μm per unit volume of the air. In Figure 1, the island and the Seoul area are
239 included in a rectangle that represents an area of interest in terms of the advection of the
240 aerosol layer. Figure 2a shows the time series of PM_{10} and $PM_{2.5}$, observed and measured
241 by the ground station on the island and a representative ground station in the Seoul area,
242 between January 10th and 19th in 2013 when there is strong advection of aerosols from East

243 Asia to the Seoul area. Around 00:00 LST on January 12th, aerosol mass starts to increase

244 and reaches its peak at 09:00 LST on January 12th on the island. Then, there is a subsequent

245 increase in aerosol mass in the Seoul area, which starts around 05:00 LST on January 12th,

246 and it reaches its peak at 18:00 LST on January 12th in the Seoul area due to the advection

247 of aerosols from East Asia to the Seoul area through the island. Figures 2b and 2c show

248 observed and measured aerosol mass distribution in the rectangle in Figure 1 at 05:00 LST

249 and 18:00 LST on January 12th, respectively. To construct Figures 2b and 2c, observed and

250 measured aerosol mass concentrations by the ground stations are interpolated into

251 equidistant points in the rectangle. Consistent with the time series, there is the high aerosol

252 mass in and around the island due to the advection of aerosols from the East-Asia continent

253 at 05:00 LST on January 12th (Figure 2b). Then, the advection continues to move aerosol

254 mass eastward further to the Seoul area, resulting in a subsequent decrease in aerosol mass

255 in and around the island and an increase in aerosol mass in the Seoul area at 18:00 LST on

256 January 12th (Figure 2c).

257   With the advection of aerosols, there is the advection of meteorological conditions.

258 To identify this advection of meteorological conditions in the Seoul area, the vertical

259 distributions of the radiosonde-observed potential temperature and humidity at 03:00 and

260 15:00 LST on January 12th in the Seoul area are obtained and shown in Figure 3. At 03:00

261 LST on January 12th just before when aerosol concentrations start to increase due to the

262 aerosol advection in the Seoul area, there is a stable layer in the PBL whose top is around

263 1.0 km (Figure 3a). This stable layer is not favorable for the formation of a deck of

264 stratiform clouds. However, after 03:00 LST on January 12th, the PBL becomes a well-

265 mixed layer and its top height increases to 1.5 km as seen in comparisons between 03:00

266 LST and 15:00 LST on January 12th in the Seoul area (Figures 3a and 3b). Hence, with

267 advection-induced increases in aerosol concentrations and the associated advection of

268 meteorological conditions, meteorological conditions become favorable for the formation

269 of a deck of stratocumulus clouds in the Seoul area. In this study, we examine how the

270 advection of aerosols affects the observed mixed-phase stratocumulus clouds in the Seoul

271 area and impacts of the advection of meteorological conditions on those clouds are out of

272 scope of this study.

273

281 **3. LES and simulations**

282

283 **3.1 LES**

284

285 As a LES Eulerian model, we use the Advanced Research Weather Research and

286 Forecasting (ARW) model (version 3.3.1), which is a nonhydrostatic compressible model

287 (Michalakes et al., 2001; Klemp et al., 2007). Prognostic microphysical variables are

288 transported with a 5th-order monotonic advection scheme (Wang et al., 2009). Shortwave

289 and longwave radiation is parameterized by the Rapid Radiation Transfer Model (RRTM;

290 Mlawer et al., 1997; Fouquart and Bonnel, 1980). The effective sizes of hydrometeors are

291 calculated in an adopted microphysics scheme and the calculated sizes are transferred to

292 the RRTM to consider effects of the effective sizes on radiation.

293 To represent microphysical processes, the LES model adopts a bin scheme based on

294 the Hebrew University Cloud Model described by Khain et al. (2011). The bin scheme

295 solves a system of kinetic equations for the size distribution functions of water drops, ice

296 crystals or cloud ice (plate, columnar and branch types), snow aggregates, graupel and hail,

297 as well as CCN and INP. Water drops whose size is smaller than 80 μm in diameter are

298 classified to be cloud droplets (or cloud liquid), while drops whose size is greater than

299 80 μm in diameter are classified to be rain drops (or rain). Each size distribution is

300 represented by 33 mass doubling bins, i.e., the mass of a particle m_k in the kth bin is

301 determined as $m_k = 2m_{k-1}$.

302 A cloud-droplet nucleation parameterization based on Köhler theory represents cloud-

303 droplet nucleation. Arbitrary aerosol mixing states and aerosol size distributions can be fed

304 to this parameterization. To represent heterogeneous ice-crystal nucleation, the

305 parameterizations by Lohmann and Diehl (2006) and Möhler et al. (2006) are used. In these

306 parameterizations, contact, immersion, condensation-freezing, and deposition nucleation

307 paths are all considered by taking into account the size distribution of INP, temperature

308 and supersaturation. Homogeneous aerosol (or haze particle) and droplet freezing is

309 also considered following the theory developed by Koop et al. (2000).

310

311 **3.2 Control run**

312

313 For a three-dimensional simulation of the observed case of mixed-phase stratocumulus

314 clouds, i.e., the control run, a domain with a 100-m resolution just over the Seoul area as

315 shown in Figure 1 is adopted. The control run is for a period between 00:00 LST on January

316 12th and 00:00 LST on January 14th in 2013. The length of the domain in the east-west

317 (north-south) direction is 220 (180) km. In the vertical domain, the resolution coarsens with

318 height. The resolution in the vertical domain is 20 m just above the surface and 100 m at

319 the model top that is at ~ 5 km in altitude.

320   Initial and boundary conditions of potential temperature, specific humidity, and

321 wind for the simulation are provided by reanalysis data. These data are produced by the

322 Met Office Unified Model (Brown et al., 2012) every 6 hours on a $0.11° \times 0.11°$ grid. These

323 data represent the synoptic-scale environment. An open lateral boundary condition is

324 employed for the control run. Surface heat fluxes are predicted by the Noah land surface

325 model (LSM; Chen and Dudhia, 2001). When clouds start to form around 08:00 LST on

326 January 12th, the average temperature over all grid points at cloud tops and bottoms is 252.0

327 and 263.9 K, respectively.

328   The horizontally homogeneous aerosol properties are assumed in the current version

329 of the ARW model. To consider the advection of aerosols and the associated

330 spatiotemporal variation of aerosol properties such as composition and number

331 concentration, this assumption of the aerosol homogeneity is abandoned. For this

332 consideration, an aerosol preprocessor is developed to represent the variability of aerosol

333 properties. Observed background aerosol properties such as aerosol mass (e.g., PM_{10} and

334 $PM_{2.5}$) at observation sites are interpolated into model grid points and time steps by this

335 aerosol preprocessor.

336   Surface sites that measure $PM_{2.5}$ and PM_{10} in the domain observe the variability of

337 aerosol properties. Here, we assume that $PM_{2.5}$ and PM_{10} represent the mass of aerosols

338 that act as CCN. These sites resolve the variability with high spatiotemporal resolutions,

339 since they are distributed with about 1 km distance between them and measure aerosol

340 mass every ~10 minutes. However, they do not measure other aerosol properties such as

341 aerosol composition and size distributions. There are additional sites of the aerosol robotic

342 network (AERONET; Holben et al., 2001) in the domain with distances of ~10 km between

343 them. Hence, these AERONET sites provide data with coarser resolutions as compared to
344 those of the $PM_{2.5}$ and PM_{10} data, although information on aerosol composition and size
345 distributions are provided by the AERONET sites. In this study, the variability of properties
346 of aerosols that act as CCN over the domain is represented by using data from the high-
347 resolution $PM_{2.5}/PM_{10}$ sites, while the relatively low-resolution data from the AERONET
348 sites are used to represent aerosol composition and size distributions.

349   According to AERONET measurements during the period with the observed
350 stratocumulus clouds, aerosol particles, on average, are an internal mixture of 70 %
351 ammonium sulfate and 30 % organic compound. This organic compound is assumed to be
352 water soluble and composed of (by mass) 18 % levoglucosan ($C_6H_{10}O_5$, density = 1600 kg
353 m^{-3}, van't Hoff factor = 1), 41 % succinic acid ($C_6O_4H_6$, density = 1572 kg m^{-3}, van't Hoff
354 factor = 3), and 41 % fulvic acid ($C_{33}H_{32}O_{19}$, density = 1500 kg m^{-3}, van't Hoff factor = 5)
355 based on a simplification of observed chemical composition. Aerosol chemical
356 composition in this study is assumed to be represented by this mixture in all parts of the
357 domain during the whole simulation period, based on the fact that aerosol composition does
358 not vary significantly over the domain during the whole period with the observed clouds.
359 Aerosols before their activation can affect radiation by changing the reflection, scattering,
360 and absorption of shortwave and longwave radiation. However, these impacts on radiation
361 are not considered in this study, since the mixture does not include a significant amount of
362 radiation absorbers such as black carbon. Based on the AERONET observation, the size
363 distribution of background aerosols acting as CCN is assumed to follow the tri-modal log-
364 normal distribution as shown in Figure 4. Stated differently, the size distribution of
365 background aerosols acting as CCN in all parts of the domain during the whole simulation
366 period is assumed to follow size distribution parameters or the shape of distribution as
367 shown in Figure 4; by averaging size distribution parameters (i.e., modal radius and
368 standard deviation of each of nuclei, accumulation and coarse modes, and the partition of
369 aerosol number among those modes) over the AERONET sites and the period with the
370 stratocumulus clouds, the assumed shape of the size distribution of background aerosols in
371 Figure 4 is obtained. Since the AERONET observation shows that the shape of the size
372 distribution does not vary significantly over the domain during the simulation period, we
373 believe that this assumption is reasonable. With the assumption above, $PM_{2.5}$ and PM_{10} are

377 converted to the background number concentrations of aerosols acting as CCN. These
378 background number concentrations, associated aerosol size distribution and composition
379 are interpolated or extrapolated to grid points immediately above the surface and time steps
380 in the simulation. Background aerosol concentrations are assumed not to vary with height
381 from immediately above the surface to the PBL top, however, above the PBL top, they are
382 assumed to reduce exponentially with height. Aerosol size distribution and composition do
383 not vary with height. Once background aerosol properties (i.e., aerosol number
384 concentrations, size distribution and composition) are put into each grid point and time step,
385 those properties at each grid point and time step do not change during the course of the
386 simulation.

387   For the control run, aerosol properties of INP and CCN are assumed to be identical
388 except for the concentration of background aerosols. The concentration of background
389 aerosols acting as INP is assumed to be 100 times lower than the concentration of
390 background aerosols acting as CCN at each of time steps and grid points. This is based on
391 a general difference in concentration between CCN and INP (Pruppacher and Klett, 1978).

392   Once clouds form and background aerosols start to be in clouds, those aerosols are
393 not background aerosols anymore and the size distribution and concentrations of those
394 aerosols begin to evolve through aerosol sinks and sources. These sinks and sources include
395 advection and aerosol activation (Fan et al., 2009). For example, activated particles are
396 emptied in the corresponding bins of the aerosol spectra. In clouds, aerosol mass included
397 in hydrometeors, after activation, is moved to different classes and sizes of hydrometeors
398 through collision-coalescence and removed from the atmosphere once hydrometeors that
399 contain aerosols reach the surface. In non-cloudy areas, aerosol size and spatial
400 distributions are set to follow background counterparts. In other words, for this study, we
401 use "the aerosol recovery method" where immediately after clouds disappear completely
402 at any grid points, aerosol size distributions and number concentrations at those points
403 recover to background properties that background aerosols at those points have before
404 those points are included in clouds. In this method, there is no time interval between the
405 cloud disappearance and the aerosol recovery. Here, when the sum of mass of all types of
406 hydrometeors (i.e., water drops, ice crystals, snow aggregates, graupel and hail) is not zero

409 at a grid point, that grid point is considered to be in clouds. When this sum becomes zero,
410 clouds are considered to disappear.

411 It is notable that in clouds, processes such as aerosol activation, which is related to
412 aerosol-cloud interactions and the nucleation scavenging, and aerosol transportation by
413 wind and turbulence, and impacts of these processes on aerosol size distribution and
414 concentrations are considered in this study as in other models that explicitly predict aerosol
415 size distribution and concentrations such as the chemistry version of the Weather Research
416 and Forecasting (WRF) model (WRF-Chem) (Grell et al., 2005; Skamarock et al., 2008).
417 When clouds disappear, in those other models, without nudging aerosols to observed
418 background counterparts, aerosols just evolve based on the emissions of aerosols around
419 the surface, aerosol chemical and physical processes, aerosol transportation and so on.
420 However, in the ARW model used here, aerosols are forced to be nudged into observed
421 background aerosols and this may act as a weakness of the aerosol recovery (or nudging)
422 method.

423 Numerous CSRM studies have adopted this aerosol recovery method and proven that
424 it is able to simulate overall cloud and precipitation properties reasonably well (e.g.,
425 Morrison and Grabowski, 2011; Lebo and Morrison, 2014; Lee et al., 2016; Lee et al.,
426 2018). These properties include cloud fraction, cloud-top height, cloud-bottom height,
427 cumulative precipitation, precipitation frequency distribution, mean precipitation rate,
428 cloud-system organization and precipitation spatiotemporal distributions. These studies
429 have shown that there is good consistency between those simulated properties and observed
430 counterparts. The good consistency means that the percentage difference in those
431 properties between simulations and corresponding observation is ~ 10 to 20% or less.

432 The recovery of aerosols to their background counterparts is mainly to keep aerosol
433 concentrations outside clouds in the simulation at observed counterparts. Other models that
434 explicitly predict aerosol concentrations with no use of the aerosol recovery method are
435 not able to simulate aerosol spatiotemporal distributions and their evolutions which are
436 identical to those observed, although those models require a much larger amount of
437 computational resources and time than the aerosol recovery method. This is mainly because
438 there are uncertainties in the representation of aerosol chemical and physical processes and
439 these processes consume a large amount of computational resources and time in those

440 models. For this study, particularly to simulate the variation of aerosol concentrations over

441 grid points and time steps induced by the aerosol advection as observed with the minimized

442 use of computational resources and time, observed aerosol concentrations, based on the

443 observed PM data and the assumed aerosol size distribution and composition, are applied

444 to grid points and time steps in the simulation directly via the aerosol preprocessor in

445 association with the aerosol recovery method. In this way, background aerosol

446 concentrations (or background aerosols or aerosols outside clouds) in the simulation are

447 exactly identical to those observed, in case we neglect possible errors from the assumption

448 on aerosol size distribution and composition, and the interpolation or extrapolation of

449 observed data to grid points and time steps in the simulation. In addition, those background

450 aerosols from observation are results of processes related to aerosols in real nature (e.g.,

451 aerosol emissions, cloud impacts on aerosols via scavenging processes, aerosol chemical

452 and physical processes and aerosol transportation by wind and turbulence). Hence, by

453 adopting background aerosols, as they are in observation, for the simulation, not only we

454 are able to consider the transportation of background aerosols by wind (or aerosol

455 advection) and associated aerosol evolutions as observed but also we are able to consider

456 the evolution of background aerosols induced by the other aerosol-related processes as

457 observed in the simulation. We believe that this balances out the weakness of the aerosol

458 recovery method to result in the reasonable simulation of the selected case, as is evidently

459 shown by the fact that simulated cloud properties are in a good agreement with observed

460 counterparts as described below.

461

462 **3.3 Additional runs**

463

464 To examine effects of the aerosol advection on the observed stratocumulus clouds over the

465 Seoul area, the control run is repeated by removing the increase in aerosol concentrations

466 due to the aerosol advection. This repeated run is referred to as the low-aerosol run.

467 In the low-aerosol run, to remove the increase in aerosol concentrations, background

468 aerosol concentrations after 05:00 LST on January 12th do not evolve with the aerosol

469 advection and are assumed to have background aerosol concentrations at 05:00 LST on

470 January 12th at every time step and grid point only for the concentration of background

473   aerosols acting as CCN. Here, the time- and domain-averaged concentration of background

474   aerosols acting as CCN after 05:00 LST on January 12th in the low-aerosol run is lower

475   than that in the control run by a factor of ~3. It is notable that there are no differences in

476   the concentration of background aerosols acting as INP between the control and low-

477   aerosol runs. This is to isolate effects of CCN, which accounts for most of aerosols, on

478   clouds from those effects of INP via comparisons between the runs. Via the comparisons,

479   we are able to identify how advection-induced increases in the concentration of aerosols

480   acting as CCN affect clouds. The ratio of the concentration of background aerosols acting

481   as CCN at 05:00 LST on January 12th to that after 05:00 LST on January 12th varies among

482   grid points and time steps, since the concentration varies spatiotemporally throughout the

483   simulation period in the control run. This means that a factor by which the concentration

484   of background aerosols acting as CCN varies after 05:00 LST on January 12th between the

485   control and low-aerosol runs is different for each of the time steps and grid points.

486   As mentioned above, impacts of the advection of meteorological conditions, which

487   accompanies the advection of aerosols and associated increases in aerosol concentrations,

488   on the stratocumulus clouds in the Seoul area are out of scope of this study. Hence, there

489   are no differences in synoptic-scale environment or meteorological conditions between the

490   control and low-aerosol runs. This enables the isolation of impacts of the aerosol advection

491   through comparisons between the runs. If impacts of the advection of meteorological

492   conditions were investigated by repeating the control run, with an assumption that

493   meteorological conditions after 03:00 LST on January 12th do not evolve and are fixed at

494   03:00 LST on January 12th, for the purpose of comparing the control run to this repeated

495   run, there would be no or nearly no formation of stratocumulus clouds in this repeated run;

496   this is because there is a stable layer at 03:00 LST on January 12th, which is just before the

497   advection of aerosols affects aerosol concentrations in the Seoul area and not favorable for

498   the formation of clouds as described in Section 2. As mentioned in Section 2, the advection

499   of meteorological conditions, which are with advection-induced increases in aerosol

500   concentrations, enables the formation of the stratocumulus clouds in the Seoul area. This

501   study examines impacts of the aerosol advection on those clouds for this given advection

502   of meteorological conditions.

503   To examine effects of the interplay between ice crystals and droplets on the adopted
504   system of stratocumulus clouds and its interactions with aerosols, the control and low-
505   aerosol runs are repeated by removing ice processes. These repeated runs are referred to as
506   the control-noice and low-aerosol-noice runs. In the control-noice and low-aerosol-noice
507   runs, only aerosols acting as CCN, droplets (i.e., cloud liquid), raindrops and associated
508   phase-transition processes (e.g., condensation and evaporation) exist, and aerosols acting
509   as INP, all solid hydrometeors (i.e., ice crystals, snow, graupel, and hail) and associated
510   phase-transition processes (e.g., deposition and sublimation) are turned off, regardless of
511   temperature. Via comparisons between the control and control-noice runs, we aim to
512   identify effects of the interplay between ice crystals and droplets on the adopted system.
513   Via comparisons between a pair of the control and low-aerosol runs and that of the control-
514   noice and low-aerosol-noice runs, we aim to identify effects of the interplay between ice
515   crystals and droplets on interactions between the system and aerosols. Henceforth, the pair
516   of the control and low-aerosol runs is referred to as the ice runs, while the pair of the
517   control-noice and low-aerosol-noice runs is referred to as the noice runs.

518   To better understand findings in Section 4.1.1, which explain how the interplay between
519   ice crystals and droplets affects stratocumulus clouds, the control run is repeated by
520   increasing the concentration of background aerosols acting as INP by a factor of 10 and
521   100 at each time step and grid point. These repeated runs are detailed in Section 4.1.2 and
522   referred to as the INP-10 and INP-100 runs, respectively. To better understand findings in
523   Section 4.2.1, which explain how aerosols acting as CCN affect the interplay between ice
524   crystals and droplets, the control run is repeated by reducing the concentration of
525   background aerosols acting as INP in the same way as the concentration of background
526   aerosols acting as CCN is reduced in the low-aerosol-run as compared to that in the control
527   run. This repeated run is referred to as the INP-reduced run and detailed in Section 4.2.2.
528   To see the roles played by the sedimentation of ice particles (i.e., ice crystals, snow
529   aggregates, graupel and hail) in stratiform clouds and their interactions with aerosols, the
530   control, INP-10, INP-100, low-aerosol and INP-reduced runs are repeated with the
531   sedimentation of ice particles turned off. These repeated runs are referred to as the control-
532   no-sedim, INP-10-no-sedim, INP-100-no-sedim, low-aerosol-no-sedim and INP-reduced-
533   no-sedim runs, and detailed in Sections 4.1.3 and 4.2.3. To examine roles played by the

sedimentation of both of ice and liquid particles (i.e., droplets and rain drops) in stratiform clouds, the control run is repeated again with the sedimentation of both of ice and liquid particles turned off. This repeated run is referred to as the control-no-sedim-ice-liq run. Table 1 summarizes all of the simulations in this study.

4. Results

4.1 Effects of the interplay between ice crystals and droplets on clouds

4.1.1 The control and control-noice runs

Figure 5a shows the time series of the domain-averaged liquid-water path (LWP), ice-water path (IWP) and water path (WP), which is the sum of LWP and IWP, for the control run, and LWP for the control-noice run. Since in the control-noice run, there are no ice particles, LWP acts as WP in the run. WP is higher in the control-noice run than in the control run throughout the whole simulation period. This higher WP in the control-noice run accompanies the higher average cloud fraction over time steps with non-zero cloud fraction. The average cloud fraction is 0.98 and 0.92 in the control-noice and control runs, respectively. At the initial stage before 20:00 LST on January 12th, differences in WP between the runs are not as significant as those after 20:00 LST on January 12th (Figure 5a). The differences in WP between the runs are greatest around 00:00 LST on January 13th when WP reaches its maximum value in each of the runs (Figure 5a). These differences decrease as time goes by after around 00:00 LST on January 13th (Figure 5a). The time- and domain-averaged WP over the period between 00:00 LST (local solar time) on January 12th and 00:00 LST on January 14th is 18 and 55 g m^{-2} in the control and control-noice runs, respectively. Associated with this, the WP peak value reaches 83 g m^{-2} in the control run, while the value reaches 230 g m^{-2} in the control-noice run (Figure 5a). Over most of the simulation period, IWP is greater than LWP in the control run except for the period between ~22:00 LST on January 12th and ~01:00 LST on January 13th (Figure 5a). In the control run, the time- and domain-averaged IWP and LWP are 11 and 7 g m^{-2}, respectively. Results here indicate that when solid and liquid particles coexist, cloud mass, represented

573   by WP, reduces a lot as compared to that when liquid particles alone exist. To evaluate the

574   control run, satellite and ground observations can be utilized. In the case of the Moderate

575   Resolution Imaging Spectroradiometer, one of representative polar orbiting image sensors

576   on board satellites, it passes the Seoul area only at 10:30 am and 1:30 pm every day, hence,

577   the sensor is not able to provide reliable data that cover the whole simulation period.

578   Multifunctional Transport Satellites (MTSAT), which are geostationary satellites and

579   available in the East Asia, do not provide reliable data of LWP and IWP, although they

580   provide comparatively reliable data of cloud fraction and cloud-top height throughout the

581   whole simulation period (Faller, 2005). Ground observations provide data of cloud fraction

582   and cloud-bottom height throughout the whole simulation period. Here, the simulated cloud

583   fraction and cloud-bottom height are compared to those from ground observations, while

584   the simulated cloud-top height is compared to that from the MTSAT. The average cloud

585   fraction over time steps with non-zero cloud fraction is 0.92 and 0.86 in the control run and

586   observation, respectively. The average cloud-bottom height over grid columns and time

587   steps with non-zero cloud-bottom height is 230 (250) m in the control run (observation).

588   The average cloud-top height over grid columns and time steps with non-zero cloud-top

589   height is 2.2 (2.0) km in the control run (observation). For this comparison between the

590   control run and observation, observation data are interpolated into grid points and time

591   steps in the control run. The percentage difference in each of cloud fraction, cloud-bottom

592   and -top heights between the control run and observations is ~ 10% and thus the control

593   run is considered performed reasonably well for these variables.

594   Condensation and deposition are the main sources of cloud mass in the control run.

595   Since in the control-noice run, there are no ice particles, deposition is absent, and thus,

596   condensation alone acts as the main source of cloud mass. As seen in Figure 5b,

597   condensation rates in the control-noice run are much higher than the sum of condensation

598   and deposition rates in the control run. Associated with this, there is greater cloud mass in

599   the control-noice run than in the control run, although deposition is absent in the control-

600   noice run. However, at the initial stage before 20:00 LST on January 12th, differences

601   between the sum in the control run and condensation rate in the control-noice run are not

602   as significant as compared to those after 20:00 LST on January 12th (Figure 5b). Hence,

603   those differences increase as time progresses after the initial stage. Those differences are

Deleted: 3

Deleted: 3

606 greatest around 00:00 LST on January 13th when the sum in the control run or condensation
607 rate in the control-noice run reaches its maximum value. The differences decrease as time
608 goes by after around 00:00 LST on January 13th. Condensation rate, deposition rate in the
609 control run, and condensation rate in the control-noice run are similar to LWP, IWP in the
610 control run, and LWP in the control-noice run, respectively, in terms of their temporal
611 evolutions (Figures 5a and 5b). This similarity confirms that deposition and condensation
612 are the main sources of IWP and LWP, respectively, and control cloud mass. Thus,
613 understanding the evolutions of condensation and deposition is equivalent to understanding
614 those of LWP and IWP, respectively. Hence, in the following, to understand evolutions of
615 cloud mass and its differences between the simulations in this study, we analyze evolutions
616 of condensation, deposition, and their differences between the runs.

617   The qualitative nature of differences in WP, which represents cloud mass, over the
618 whole simulation period between the control and control-noice runs is initiated and
619 established during the initial stage of cloud development before 20:00 LST on January 12th
620 (Figures 5a and 5b). Hence, to understand mechanisms that initiate differences in WP
621 between the control and control-noice runs, deposition, condensation and associated
622 variables are analyzed for the initial stage. Note that synoptic or environmental conditions
623 such as humidity and temperature are identical between the control and control-noice runs.
624 These conditions act as initial and boundary conditions for the simulations and thus initial
625 and boundary conditions are identical between the runs. Also, during the initial stage,
626 feedbacks between dynamics (e.g., updrafts) and microphysics just start to form and thus
627 are not fully established as compared to those feedbacks after the initial stage. This enables
628 us to perform analyses of deposition and condensation during the initial stage by reasonably
629 excluding a large portion of complexity caused by those feedbacks. Hence, those analyses
630 during the initial stage can provide a clearer picture of either microphysical or dynamic
631 mechanisms that control differences in results between the runs.

632   During the initial stage before 20:00 LST on January 12th, evaporation rates, averaged
633 over the cloud layer, are higher in the control run than in the control-noice run and this is
634 contributed by the WBF mechanism which facilitates evaporation of droplets and
635 deposition onto ice crystals (Figure 5c). In addition, it should be noted that ice crystals
636 consume water vapor that is needed for droplet nucleation. This makes it difficult for

Deleted: 3
Deleted: 3
Deleted: 3
Deleted: 3
Deleted: 3

642 droplets to be activated in the control run as compared to a situation in the control-noice
643 run. Associated with the more evaporation and difficulty in droplet activation, droplets
644 disappear more and form less, leading to a situation where cloud droplet number
645 concentration (CDNC) starts to be lower in the control run during the initial stage (Figure
646 5d). This is despite the higher entrainment rate at the PBL tops and associated more
647 evaporation in the control-noice run than in the control run. The average entrainment rate
648 over all grid points at the PBL tops and over the initial stage is 0.18 and 0.08 cm s^{-1} in the
649 control-noice and control runs, respectively. In this study, the entrainment rate is calculated
650 as follows:

651

652 *The entrainment rate = $dz_i/dt - w_{sub}$*

653

654 Here, z_i is the PBL height and w_{sub} is the large-scale subsidence rate at the PBL top. Then,
655 during the initial stage, the reduction in CDNC contributes to a reduction in condensation
656 in the control run as compared to that in the control-noice run (Figure 5b). Fewer droplets
657 mean that there is a less integrated droplet surface area where condensation occurs and this
658 contributes to less condensation in the control run. As seen in Figures 5c and 5d, the cloud
659 layer is between ~200 m and ~1.5 km in the control run, while it is between ~200 m and
660 ~2.5 km in the control-noice run. Hence, air parcels go up higher, which also contribute to
661 more condensation in the control-noice run than in the control run. However, aided by the
662 fact that the water-vapor equilibrium saturation pressure is lower for ice particles than for
663 liquid particles, deposition is facilitated at the initial stage in the control run whether the
664 water-vapor pressure is higher than the equilibrium pressure for liquid particles or not as
665 long as the water-vapor pressure is higher than the equilibrium pressure for ice particles.
666 This leads to greater deposition than condensation in the control run at the initial stage
667 (Figure 5b). This deposition is inefficient and the subsequent increase in deposition is not
668 sufficient, so, the sum of condensation and deposition rates in the control run is slightly
669 lower than condensation rate in the control-noice run at the initial stage (Figure 5b); this
670 contributes to slightly lower WP in the control run than in the control-noice run during the
671 initial stage (Figure 5a). Hence, slightly greater latent heating, which is associated with
672 condensation, in the control-noice run than that, which is associated with the sum of

Deleted: 3

Deleted: As seen in Figure 3c, the cloud layer is between ~200 m and ~1.5 km in the control run, while it is between ~200 and ~2.5 km in the control-noice run.

Deleted: 3

Deleted: It should be noted that as seen in Figures 3c and 3d

Deleted: 3

Deleted: 3

Deleted: 3

682   deposition and condensation, in the control run develops during the initial stage. This

683   initiates stronger feedbacks between updrafts and latent heating in the control-noice run

684   than in the control run during the initial stage and these stronger feedbacks are fully

685   established after the initial stage. This in turn results in much stronger updrafts after the

686   initial stage in the control-noice run than in the control run. Mainly due to these much

687   stronger updrafts after the initial stage, the time- and domain-averaged updrafts over the

688   whole simulation period are also much greater in the control-noice run than in the control

689   run (Figure 6a). The much stronger updrafts produce much larger WP and associated larger

690   cloud fraction in the control-noice run than in the control run after the initial stage (Figure

691   5a).

692   Results here indicate that the reduced cloud mass, due to the reduced condensation,

693   is not efficiently compensated by the gain of solid mass via deposition in the control run.

694   If the reduced mass is efficiently compensated by deposition, that would lead to much

695   smaller differences in WP between the control and control-noice runs. Here, we

696   hypothesize that the inefficient deposition is related to cloud ice number concentration

697   (CINC) as seen in Figure 6b. Note that the surface of ice crystals is where deposition occurs

698   and the more surface area of ice crystals favors more deposition. We hypothesize that CINC

699   and the associated integrated surface area of ice crystals are not large enough to induce a

700   large amount of deposition that can potentially make WP similar between the control and

701   control-noice runs. Stated differently, it is hypothesized that water vapor is not able to find

702   enough surface area of ice crystals for the large amount of deposition.

703

704   **a. LWP and IWP frequency distributions**

705

706   As seen in Figure 7a, the control-noice run has the lower (higher) WP cumulative frequency

707   for WP below (above) ~ 100 g m^{-2} than the control run at the last time step. This means

708   that the lower average WP in the control run is mainly due to a reduction in WP above

709   ~ 100 g m^{-2} in the control run. The LWP frequency reduces substantially in the control run

710   as compared to that in the control-noice run (Figure 7b). With this reduction, LWP above

711   ~ 800 g m^{-2} disappears and there is in general two to three orders of magnitude lower LWP

Deleted: 4

Deleted: 3

Deleted:

Deleted: 4

Deleted: T

Deleted: area

Deleted: 5

Deleted: 5

720 frequency for LWP below ~ 800 g m^{-2} in the control run than in the control-noice run

721 (Figure 7b).

722 As seen in Figure 7b, at the last time step, there is the presence of IWP frequency in

723 addition to the LWP frequency in the control run. Through the facilitated deposition, the

724 IWP frequency is greater than the LWP frequency for IWP below ~ 200 g m^{-2} in the control

725 run. Particularly for IWP below ~ 100 g m^{-2}, the IWP frequency in the control run is greater

726 than the LWP frequency in the control-noice run. This enables the greater WP frequency

727 in the control run than in the control-noice run for WP below ~ 100 g m^{-2} in spite of the

728 lower LWP frequency below ~100 g m^{-2} in the control run (Figures 7a and 7b). However,

729 the lower IWP frequency for IWP above ~ 100 g m^{-2} in the control run than the LWP

730 frequency for LWP above ~ 100 g m^{-2} in the control-noice run contributes to the lower WP

731 frequency for WP above ~ 100 g m^{-2} in the control run (Figures 7a and 7b). The lower WP

732 frequency for WP above ~ 100 g m^{-2} in the control run is also contributed by the lower

733 LWP frequency for LWP above ~ 100 g m^{-2} in the control run (Figures 7a and 7b).

734

735 **4.1.2 The INP-10 and INP-100 runs**

736

737 To test above-mentioned hypothesis about the CINC-related inefficient deposition, the

738 control run is compared with the INP-10 and INP-100 runs (Table 1). In particular, in the

739 INP-100 run, the concentration of background aerosols acting as INP becomes that of

740 background aerosols acting as CCN. This may be unrealistic. However, the main purpose

741 of the INP-10 and INP-100 runs is to test the hypothesis and it is believed that the high

742 concentrations of background aerosols acting as INP in the INP-10 and INP-100 runs are

743 able to clearly isolate the role of the INP concentration and CINC in WP by making a stark

744 contrast in the INP concentration and CINC between the control, INP-10 and INP-100 runs.

745 As seen in Figure 8a, CINC averaged over grid points and time steps with non-zero

746 CINC increases by a factor of ~5 (~60), when the concentration of background aerosols

747 acting as INP increases by a factor of 10 (100) from the control run to the INP-10 (INP-

748 100) run. With these increases in CINC, the average radius of ice crystals over grid points

749 and time steps with non-zero CINC decreases by ~15% and 25% in the INP-10 and INP-

750 100 runs, respectively. This induces increases in the integrated surface area of ice crystals

Deleted: 5

Deleted: 5

Deleted: 5

Deleted: 5

Deleted: 5

Deleted: 5

Deleted: 5

Deleted: 5

Deleted: 6

and thus deposition in the INP-10 and INP-100 runs as compared to those in the control run (Figures 5b, 8b and 8c). These increases in deposition are more, because of greater increases in the integrated surface area in the INP-100 run than in the INP-10 run (Figures 8b and 8c). Of interest is that the increase in deposition accompanies a decrease in condensation in the INP-10 and the INP-100 runs as compared to that in the control run (Figures 5b, 8b and 8c). This is because due to more deposition, more water vapor is transferred from air to ice crystals, which leaves less water vapor for droplet activation and condensation in the INP-10 run and INP-100 runs than in the control run when the water-vapor pressure is higher than the water-vapor saturation pressure for liquid particles in air parcels. Greater deposition leaves less water vapor for droplet activation and condensation, leading to less activation and condensation in the INP-100 run than in the INP-10 run when the water-vapor pressure is higher than the water-vapor saturation pressure for liquid particles in air parcels. When the water-vapor pressure is lower than the water-vapor saturation pressure for liquid particles, increasing deposition induces the increasing evaporation of droplets and decreasing CDNC among the control, INP-10 and INP-100 runs in air parcels. This subsequently contributes to decreasing condensation among those runs when the water-vapor pressure becomes higher than the water-vapor saturation pressure for liquid particles in those air parcels.

Associated with increases in deposition and decreases in condensation, IWP increases and LWP decreases in both of the INP-10 and INP-100 runs as compared to those in the control run. The time- and domain-averaged IWP, LWP and WP are 24 (47), 5 (3), and 29 (50) g m^{-2} in the INP-10 (INP-100) run. Since there are greater increases in deposition and greater decreases in condensation, these increases in IWP and decreases in LWP are greater in the INP-100 run than in the INP-10 run. The increasing deposition and IWP contribute to increases in WP, while the decreasing condensation and LWP contribute to decreases in WP in the INP-10 and INP-100 runs. Figure 9a shows that there are increases in WP in the INP-10 and INP-100 runs as compared to WP in the control run and those increases are greater in the INP-100 run than in the INP-10 run. This means that the increases in deposition and IWP outweigh the decreases in condensation and LWP, respectively, in the INP-10 and INP-100 runs. This outweighing is greater and leads to greater increases in WP in the INP-100 run than in the INP-10 run (Figure 9a). As seen in Figure 9a, the enhanced

802 average WP in the INP-100 (INP-10) run reaches 91% (53%) of that in the control-noice

803 run, while the average WP in the control run accounts for only ~30% of that in the control-

804 noice run. Associated with the enhanced average WP, the average cloud fraction over time

805 steps with non-zero cloud fraction increases from 0.92 in the control run to 0.97 (0.94) in

806 the INP-100 (INP-10) run. Accompanying this is that the time- and domain-averaged

807 updraft mass flux in the INP-100 (INP-10) run over the whole simulation period reaches

808 95% (78%) of that in the control-noice run, while the average updraft mass flux in the

809 control run accounts for only ~50% of that in the control-noice run. The average cloud-top

810 height over grid columns and time steps with non-zero cloud-top height in the INP-100

811 (INP-10) run, particularly over the initial stage between 00:00 LST and 20:00 LST on

812 January 12th, reaches 92% (80%) of that in the control-noice run. Hence, the increasing

813 deposition in the INP-10 and INP-100 runs involves its positive feedbacks with dynamics

814 (i.e., updrafts). This eventually enables air parcels in the INP-100 run to have stronger

815 updrafts than those in the control run and thus to go up nearly as high as those in the control-

816 noice run. Through the positive feedbacks between the increasing deposition and dynamics,

817 increasing dynamic intensity with the increasing vertical extent of air parcels or clouds in

818 turn enables deposition and IWP to further increase, resulting in the similar WP and cloud

819 fraction between the INP-100 and control-noice runs. Here, comparisons among the control,

820 INP-10 and INP-100 runs confirm the hypothesis that ascribes much lower WP in the

821 control run than in the control-noice run to the CINC-related inefficient deposition in the

822 control run.

823

824   **a. LWP and IWP frequency distributions**

825

826 With the increasing concentration of aerosols acting as INP and CINC from the control run

827 to the INP-10 run to the INP-100 run, there are substantial increases in the IWP cumulative

828 frequency, while there are substantial decreases in the LWP cumulative frequency at the

829 last time step (Figure 9b). These increases in the IWP frequency accompany increases in

830 the IWP maximum value from ~200 g m^{-2} in the control run to ~1200 g m^{-2} in the INP-100

831 run through ~500 g m^{-2} in the INP-10 run (Figure 9b). These decreases in the LWP

832 frequency accompany decreases in the LWP maximum value from ~700 g m^{-2} in the control

Deleted: .

Deleted: .

Deleted:

Deleted: and

Deleted: t

Deleted: in the INP-100 run

Deleted:

Deleted:

Deleted: 7

Deleted: 7

843 run to ~100 g m^{-2} in the INP-100 run through ~300 g m^{-2} in the INP-10 run (Figure 9b).

844 The increases in the IWP frequency outweigh decreases in the LWP frequency between the

845 INP-10 and INP-100 runs (the INP-10 and control run), leading to the greater average WP

846 in the INP-100 run than in the INP-10 run (in the INP-10 run than in the control run).

847

848 **4.1.3 Sedimentation of hydrometeors**

849

850 With increasing concentrations of aerosols acting as INP between the control, INP-10 and

851 INP-100 runs, there are changes in the sedimentation of ice particles and this induces

852 changes in the precipitation rate at cloud bases. The average precipitation rate over all grid

853 points at cloud bases and over the whole simulation period is 0.004, 0.002, and 0.0006 g

854 m^{-2} s^{-1} in the control, INP-10 and INP-100 runs, respectively. As mentioned above, there

855 are also changes in the deposition rate among those simulations. The time- and column-

856 averaged deposition rate is 0.027, 0.059 and 0.125 g m^{-2} s^{-1} in the control, INP-10 and INP-

857 100 runs, respectively. As a first step to obtain the column average of a variable, at each

858 time step, the average value of the variable over each column is obtained by summing up

859 the value of the variable over the vertical domain in each of all columns in the domain and

860 dividing the sum by the total number of gird points in each column. This sum of the value

861 is obtained over all grid points in the vertical domain whether they have zero values of the

862 variable or not. The column average in this study is the average value (in each column) that

863 is summed up over all columns and divided by the total number of columns in the domain.

864 We see that the change in deposition rate from the control run to the INP-10 run (to the

865 INP-100 run) is 16 (29) times greater than that in the cloud-base precipitation rate. Hence,

866 the varying sedimentation of ice particles and associated precipitation is likely to play an

867 insignificant role in the varying cloud mass among the runs as compared to the varying

868 deposition. To confirm this, the control, INP-10 and INP-100 runs are repeated by setting

869 the fall velocity of ice particles to zero. These repeated runs are the control-no-sedim and

870 INP-10-no-sedim and INP-100-no-sedim runs. The time- and domain-averaged IWP, LWP

871 and WP are 11 (14), 7 (5) and 18 (19) g m^{-2}, respectively, in the control (control-no-sedim)

872 run. The time- and domain-averaged IWP, LWP and WP are 26 (49), 4 (2) and 30 (51) g

873 m^{-2}, respectively, in the INP-10-no-sedim (INP-100-no-sedim) run. Remember that the

Deleted: 7

Deleted: ice particles

time- and domain-averaged IWP, LWP and WP are 24 (47), 5 (3) and 29 (50) g m^{-2}, respectively, in the INP-10 (INP-100) run. The presence of the sedimentation decreases IWP and increases LWP as compared to the situation with no sedimentation for each of the runs. However, the average WP in the control-no-sedim run is still much lower than that in the control-noice run. The average WP in the INP-100-no-sedim run (the INP-10-no-sedim run) reaches 93% (55%) of that in the control-noice run and this is similar to the situation among the INP-10, INP-100 and control-noice runs. This demonstrates that the sedimentation of ice particles and associated precipitation are not main factors that control the variation of cloud mass among the control, INP-10, INP-100 and control-noice runs.

To further examine the role played by the sedimentation of hydrometeors particularly in the lower WP in the control run than that in the control-noice run, the control run is repeated again by setting the fall velocity of both of ice and liquid particles to zero. The repeated run is the control-no-sedim-ice-liq run. The time- and domain-averaged IWP, LWP and WP are 11 (15), 7 (9) and 18 (24) g m^{-2}, respectively, in the control (control-no-sedim-ice-liq) run. The presence of the sedimentation of both of ice and liquid particles decreases both of IWP and LWP as compared to the situation with no sedimentation of both of ice and liquid particles. However, the average WP in the control-no-sedim-ice-liq run is still much lower than that in the control-noice run. Hence, the lower WP in the control run than that in the control-noice run does not depend on whether the sedimentation of both of ice and liquid particles is present in the control run. This indicates that the sedimentation of both of ice and liquid particles is not a factor that causes the lower WP in the control run than in the control-noice run.

4.2 Aerosol-cloud interactions

4.2.1 CCN

With advection-induced increases in aerosol concentrations between the control and low-aerosol runs, there are aerosol-induced increases and decreases in IWP and LWP, respectively (Figure 10a). The increases in IWP are outweighed by the decreases in LWP, leading to aerosol-induced decreases in the average WP between the ice runs. This involves

aerosol-induced decreases in the average cloud fraction over time steps with non-zero cloud fraction from 0.93 in the low-aerosol run to 0.92 in the control run. As seen in Figure 10b, the WP frequency is greater particularly for WP < ~300 g m^{-2}, leading to the higher average WP in the low-aerosol run than in the control run. As seen in Figure 10c, particularly for WP below ~200 g m^{-2}, the IWP frequency increases, while the LWP frequency decreases with increasing aerosols between the ice runs. The increase in the IWP frequency is not able to outweigh the decrease in the LWP frequency, leading to aerosol-induced decreases in the average WP between the ice runs. Results here are contrary to the conventional wisdom that increasing concentrations of aerosols acting as CCN tend to increase WP in stratiform clouds (Albrecht, 1989).

Between the noice runs, there is an increase in LWP (i.e., WP) with the increasing concentration of aerosols acting as CCN (Figure 10a). This involves aerosol-induced increases in the average cloud fraction over time steps with non-zero cloud fraction from 0.96 in the low-aerosol-noice run to 0.98 in the control-noice run. The greater LWP frequency, concentrated in the LWP range between ~100 and ~600 g m^{-2}, leads to the greater average LWP or WP in the control-noice run than in the low-aerosol-noice run (Figures 10b and 10c).

a. Ice runs

   1) Condensation and evaporation

The qualitative nature of aerosol-induced differences in deposition, IWP, condensation and LWP over the whole simulation period between the ice runs is initiated and established during the initial stage of cloud development before 20:00 LST on January 12th (Figure 10a). To understand mechanisms that control aerosol-induced differences in deposition and condensation as a way of understanding mechanisms that control those differences in IWP and LWP, the time series of deposition rate, condensation rate and associated variables in each of the ice runs and differences in these variables between the ice runs is obtained for the initial stage. Since this study focuses on these differences in the variables as a representation of aerosol effects on clouds, in the following, the description of the

Deleted: 8

Deleted: 8

Deleted: 8

Deleted: 8

Deleted: 8

Deleted: 8

949   differences is given in more detail by involving both figures and text as compared to the

950   description of the variables in each of the ice runs, involving text only for the sake of

951   brevity.

952

953   i.   CDNC and its relation to condensation and evaporation

954

955   Evaporation and condensation rates are higher in the control run than in the low-aerosol

956   run throughout the initial stage and up to ~15:30 LST on January 12th, respectively (Figure

957   11a). Increases in evaporation tend to make more droplets disappear, while increases in

958   aerosol activation and resultant condensation counteract the disappearance more. The

959   average CDNC over grid points and time steps with non-zero CDNC is larger in the control

960   run than in the low-aerosol run not only over the initial stage but also over the whole

961   simulation period (Figures 11a and 12a). This means that on average, the evaporatively-

962   driven increases in the disappearance of droplets are outweighed by the activation- and/or

963   condensationally-enhanced counteraction particularly during the initial stage with

964   increasing aerosol concentrations between the ice runs. As marked by a green-dashed box

965   in Figure 11a, there are steady and rapid temporal increases in the CDNC differences

966   between the ice runs over a period from 12:50 to 13:20 LST on January 12th. This is due to

967   steady and rapid temporal increases in CDNC, which are larger in the control run than in

968   the low-aerosol run, over the period. More droplets or higher CDNC provides a larger

969   integrated surface area of droplets where evaporation and condensation of droplets occur,

970   and thus acts as more sources of evaporation and condensation. With steady and rapid

971   temporal increases in CDNC as a source of evaporation and condensation, temporal

972   increases in both evaporation and condensation show a jump (or a surge or a rapid increase)

973   in them for the period between 12:50 and 13:20 LST on January 12th in each of the ice runs

974   (Supplementary Figure 1). Here, evaporation occurs at grid points where the water-vapor

975   pressure is lower than the water-vapor equilibrium saturation pressure for liquid particles

976   and thus WBF mechanism can occur, while condensation occurs at grid points where the

977   water-vapor pressure is higher than the water-vapor equilibrium saturation pressure for

978   liquid particles. This jump is higher associated with the larger temporal increase in CDNC

979   in the control run than in the low-aerosol run (Supplementary Figure1). This induces

984 differences in each of evaporation and condensation between the ice runs to jump, as also

985 marked by the green-dashed box in Figure 11a, during the time period.

986   The jump in differences in condensation between the ice runs is not as high as that in

987 differences in evaporation between the ice runs (Figure 11a). This situation accompanies

988 the fact that in each of the ice runs, the jump in evaporation is higher than that in

989 condensation (Supplementary Figure 1). This means that differences in the jump between

990 evaporation and condensation are greater in the control run than in the low-aerosol run

991 (Supplementary Figure 1). Hence, evaporation-driven jump in the disappearance of

992 droplets outweighs condensation-driven jump in counteraction against the disappearance

993 in each of the ice runs. Due to this, the increasing temporal trend of CDNC turns to its

994 decreasing trend in each of the ice runs around 13:30 LST on January 12th. If the rate of

995 this decrease in CDNC with time is equal between the ice runs, there is no decreasing trend

996 in differences in CDNC between the runs. However, remember that differences in the jump

997 between evaporation and condensation are greater in the control run than in the low-aerosol

998 run. Hence, when the jumps occur, evaporation-induced disappearance of droplets is

999 counteracted by condensation "less" in the control run than in the low-aerosol run. This

1000 induces the rate of the CDNC decrease to be greater in the control run than in the low-

1001 aerosol run. This in turn turns the increasing temporal trend of the CDNC differences

1002 between the ice runs to their decreasing trend around 13:30 LST on January 12th (Figure

1003 11a).

1004   The decreasing temporal trend of CDNC contributes to a decreasing temporal trend

1005 of each evaporation and condensation, starting around 13:30 LST on January 12th, by

1006 reducing the integrated surface area of droplets in each of the ice runs. This decreasing

1007 trend of each evaporation and condensation is larger associated with the larger decreasing

1008 trend of CDNC in the control run than in the low-aerosol run (Supplementary Figure 1).

1009 This induces the increasing temporal trend of differences in each evaporation and

1010 condensation between the ice runs to change into their decreasing temporal trend around

1011 13:30 LST on January 12th (Figure 11a). The decreasing trend of evaporation in each of the

1012 ice runs is smaller than that in condensation (Supplementary Figure 1). Associated with

1013 this, the decreasing trend of differences in evaporation between the ice runs is smaller than

1014 that in condensation (Figure 11a). Stated differently, the temporal reduction in evaporation

1020 in each of the ice runs and its differences between the runs from 13:30 LST on January 12th

1021 onwards during the initial stage occurs to a less extent as compared to that in condensation

1022 and its differences.

1023

1024   ii.   Evaporation and condensation efficiency

1025

1026 For a given humidity, the increase in the surface-to-volume ratio of droplets increases the

1027 evaporation (condensation) efficiency by increasing the integrated surface area of droplets

1028 per unit volume or mass of droplets. Here, evaporation (condensation) efficiency is defined

1029 to be the mass of droplets that are evaporated (condensed) per unit volume or mass of

1030 droplets. Aerosol-induced increases in the surface-to-volume ratio and thus evaporation

1031 and condensation efficiency are caused by aerosol-induced increases in CDNC and

1032 associated decreases in the droplet size. Increasing CDNC, in turn, increases competition

1033 among droplets for given water vapor needed for their condensational growth, leading to

1034 decreases in the droplet size. The average droplet radius over grid points and time steps

1035 with non-zero CDNC is 7.3, 9.8, 8.7, and 10.5 μm in the control, low-aerosol, control-noice

1036 and low-aerosol-noice runs, respectively. It is notable that the WBF-mechanism-induced

1037 evaporation per unit volume of droplets when the water-vapor pressure is lower than or

1038 equal to the water-vapor equilibrium saturation pressure for liquid particles but higher than

1039 the equilibrium pressure for ice particles is also strongly proportional to the surface-to-

1040 volume ratio of droplets (Pruppacher and Klett, 1978). Hence, between the ice runs,

1041 enhanced evaporation efficiency by aerosol-induced increases in the surface-to-volume

1042 ratio accompanies aerosol-enhanced WBF-mechanism-associated efficiency of

1043 evaporation in addition to aerosol-enhanced efficiency of evaporation when the water-

1044 vapor pressure is lower than the water-vapor equilibrium pressure for ice particles.

1045   With the steady and rapid temporal increase in CDNC, there is a steady and rapid

1046 temporal enhancement of the surface-to-volume ratio of droplets and evaporation

1047 efficiency in each of the ice runs between 12:50 and 13:20 LST on January 12th. Remember

1048 that these increases in CDNC are larger in the control run than in the low-aerosol run. This

1049 induces the greater temporal enhancement of the ratio and evaporation efficiency in the

1050 control run than in the low-aerosol run. The temporal enhancement of the ratio and

evaporation efficiency accompanies the temporally enhancing WBF-mechanism-related efficiency of evaporation. This accompaniment boosts evaporation and enables the jump in temporal increases in evaporation to be greater than that in condensation in each of the ice runs. In association with the larger steady and rapid temporal increase in CDNC in the control run than in the low-aerosol run, the temporally enhancing WBF-mechanism-related efficiency of evaporation and its boost on evaporation enhance with increasing aerosol concentrations. This, in turn, enables greater aerosol-induced increases in evaporation than in condensation or the greater jump in differences in evaporation between the ices runs than that in condensation over the period between 12:50 and 13:20 LST on January 12th (Figure 11a). For the period between 12:50 and 13:20 LST, there is no steady and rapid temporal increase in differences in the entrainment rate at the PBL tops unlike the situation with CDNC differences between the ice runs (Figure 11b). Hence, the greater jump in differences in evaporation between the ice runs is not likely to be induced by entrainment.

Even when both evaporation and condensation rates decrease with time in association with the decreasing temporal trend of CDNC and the surface-to-volume ratio of droplets over a period after 13:30 LST on January 12th during the initial stage in each of the ice runs, evaporation (condensation) rates are maintained higher throughout the initial stage (up to ~15:30 LST) in association with the higher CDNC and surface-to-volume ratio of droplets in the control run than in the low-aerosol run (Figure 11a). The presence of the WBF mechanism and entrainment facilitates evaporation and this acts against the temporal decrease in evaporation with time over the period in each of the ice runs. This counteraction by the WBF mechanism and entrainment reduces the temporal decrease in evaporation and enables evaporation to reduce temporally to a less extent as compared to condensation in each of the ice runs for the period (Supplementary Figure 1). This accompanies the differences in the temporal reduction between evaporation and condensation that are larger in the control run than in the low-aerosol run (Supplementary Figure 1). This, in turn, enables differences in evaporation between the ice runs to reduce to a less extent as compared to those in condensation over the period (Figure 11a). Due to this, differences (or aerosol-induced increases) in evaporation and associated aerosol-induced increases in evaporation-driven negative buoyancy between the ice runs are higher than those in condensation and condensation-driven positive buoyancy, respectively, for the period

Deleted: 9

Deleted: 9

Deleted: 9

Deleted: 9

(Figure 11a). This induces the decreasing temporal trend of differences or aerosol-induced increases in updraft mass fluxes between the ice runs over the period (Figure 11a). The decreasing temporal trend of aerosol-induced increases in updraft mass fluxes eventually leads to lower updraft mass fluxes in the control run than in the low-aerosol run, as represented by negative differences in updraft mass fluxes between the ice runs from ~15:30 LST onwards during the initial stage (Figure 11a). Associated with this, condensation becomes smaller in the control run, as represented by negative differences in condensation between the ice runs from ~15:30 LST onwards during the initial stage (Figure 11a).

The role of the WBF mechanism described in this section can be clearly seen by comparing the ice runs in this section to the noice runs, with no WBF mechanism, detailed in the following Section b.

2) Deposition and condensation

The difference in deposition between the ice runs is negligible and does not vary much with time up to ~15:30 LST on January 12th when the difference starts to show its significant increase (Figure 11a). With the start of the decreasing temporal trend of condensation around 13:30 LST on January 12th, more water vapor, not used by condensation, becomes available for deposition as compared to that before 13:30 LST on January 12th in each of the ice runs. Remember that this decreasing trend is greater in the control run than in the low-aerosol run. Hence, from 13:30 LST on January 12th onwards, more water vapor is available for deposition in the control run than in the low-aerosol run. This leads to the start of larger aerosol-induced increases in deposition between the ice runs around 13:30 LST on January 12th as compared to those increases before ~ 13:30 LST on January 12th (Figure 11a). The decrease in condensation in the control run continues and its differences between the runs grow even after the negative differences in condensation between the runs start to appear around 15:30 LST on January 12th. Hence, aerosol-induced increases in the amount of water vapor, which is not used by condensation and available for deposition, continue even after 15:30 LST on January 12th. This enables aerosol-induced increases in deposition between the ice runs to continue even after 15:30 LST on

Deleted: 9

Deleted: 9

Deleted: 9

Deleted: 9

Deleted: 9

Deleted: 9

January 12th (Figure 11a). This is despite the evaporation-driven lower updraft mass fluxes in the control run than in the low-aerosol run from ~ 15:30 LST on January 12th onwards (Figure 11a). This indicates that after ~ 15:30 LST on January 12th, the microphysical process which is related to the competition between deposition and condensation and tends to increase deposition with increasing aerosol concentrations outweighs dynamic processes (i.e., updraft mass fluxes) which tend to reduce deposition with increasing aerosol concentrations.

The increasing temporal trend of aerosol-induced increases in deposition is not able to outweigh the increasing trend of aerosol-induced decreases in condensation between the ice runs after ~ 15:30 LST on January 12th (Figure 11a). Remember that there is no change in the background concentration of aerosols acting as INP between the ice runs. Hence, as seen in Figure 11a, there are negligible differences in CINC between the ice runs, although more water vapor starts to be available for deposition in the control run than in the low-aerosol run around 13:30 LST on January 12th. This indicates that CINC per unit water vapor available for deposition is lower in the control run. Hence, the available water vapor has more difficulty in finding the surface area of ice crystals for deposition in the control run. The more difficulty in finding the surface area of ice crystals for deposition makes the deposition of the more available water vapor less efficient in the control run than in the low-aerosol run. This damps down the increase in deposition particularly after ~ 13:30 LST on January 12th in the control run. Then, aerosol-induced increases in deposition are not large enough to overcome aerosol-induced decreases in condensation in the control run particularly after ~ 15:30 LST on January 12th (Figure 11a). This in turn leads to the lower average WP in the control run than in the low-aerosol run over the whole simulation period.

b. Noice runs

As between the ice runs, between the noice runs, the activation- and condensationally-enhanced counteraction outweighs the evaporation-induced decreases in CDNC, leading to increases in CDNC with increasing aerosol concentrations (Figures 11a, 11c, and 12b). However, in the noice runs, ice processes, the associated WBF mechanism and increase in the WBF-mechanism-associated efficiency of evaporation with increasing aerosol

1162   concentrations are absent, although aerosol-induced increases in entrainment at the PBL

1163   tops and surface-to-volume ratio of droplets are present. The average entrainment rate over

1164   all grid points at the PBL tops and over the whole simulation period is 0.71 and 0.60 cm s$^-$

1165 ^{1} in the control-noice and low-aerosol-noice runs, respectively. The average entrainment

1166   rate over all grid points at the PBL tops and over the whole simulation period is 0.13 and

1167   0.15 cm s^{-1} in the control and low-aerosol runs. There are aerosol-induced decreases in the

1168   average entrainment over the whole simulation period between the ice runs. The boost of

1169   evaporation by the WBF mechanism in each of the ice runs leads to greater evaporation

1170   efficiency by outweighing the lower entrainment rate in the control run than in the control-

1171   noice run and in the low-aerosol run than in the low-aerosol-noice run. Aerosol-induced

1172   increases in the boost lead to aerosol-induced greater increases in evaporation efficiency

1173   between the ice runs than between the noice runs despite aerosol-induced decreases

1174   (increases) in the entrainment rate between the ice (noice) runs for the whole simulation

1175   period. Particularly for the initial stage, evaporation efficiency in the control, low-aerosol,

1176   control-noice, and low-aerosol-noice runs is 1.61, 0.90, 0.21, and 0.12 %, respectively.

1177   Here, to obtain evaporation efficiency, the cumulative values of evaporation and cloud-

1178   liquid mass at the last time step of the initial stage are calculated as follows:

1179

1180   *A cumulative value of an arbitrary variable "A"* $= \iint A dV dt$ (1)

1181

1182   Here, $dV = dxdydz$ and t represents time. x, y and z represent displacement in east-west,

1183   north-south and vertical directions, respectively. Evaporation rate in a unit volume of air,

1184   which is in a unit of kg m^{-3} s^{-1}, at each grid point and time step is put into Eq. (1) as "A" to

1185   obtain the cumulative value of evaporation. To obtain the cumulative value of cloud-liquid

1186   mass, cloud-liquid mass in a unit volume of air at each grid point and time step is first

1187   divided by the time step. This divided cloud-liquid mass, which is also in a unit of kg m^{-3}

1188   s^{-1}, represents cloud-liquid mass per unit time and volume and is put into Eq. (1) as "A" to

1189   obtain the cumulative value of cloud-liquid mass. Then, the cumulative evaporation is

1190   divided by the cumulative cloud-liquid mass to obtain the evaporation efficiency for each

1191   of the runs.

Field Code Changed

With temporal increases in CDNC, which are larger in the control-noice run than in the low-aerosol-noice run, leading to those in CDNC differences between the noice runs, there are temporal increases in condensation and evaporation, which are larger in the control-noice run than in the low-aerosol-noice run, and thus in their differences between the noice runs (Figure 11c). Associated with aerosol-induced smaller increases in evaporation efficiency between the noice runs, aerosol-induced increases in condensation are always greater than aerosol-induced increases in evaporation between the noice runs during the initial stage (Figure 11c). This maintains aerosol-induced increases in updraft mass fluxes between the noice runs and leads to aerosol-induced increases in WP between the noice runs. Also, with higher CDNC and associated smaller sizes of droplets, there is suppressed autoconversion in the control-noice run as compared to that in the low-aerosol-noice run. Here, autoconversion is the process of droplets colliding with and coalescing each other to grow into raindrops. Due to this, the average precipitation rate over all grid points at cloud bases and over the whole simulation period is lower in the control-noice run. The average cloud-base precipitation rate is 0.009 and 0.019 g m^{-2} s^{-1} in the control-noice and low-aerosol-noice runs, respectively. The difference in this average precipitation rate between the noice runs is ~ two times smaller than that in the time- and column-averaged condensation rate. Hence, while aerosol-induced precipitation suppression contributes to higher WP in the control-noice run, this contribution is not as significant as that of aerosol-enhanced condensation.

In contrast to the situation in the noice runs, in the ice runs, after ~12:50 LST on January 12th, aerosol-induced increases in condensation become lower than those in evaporation, leading to aerosol-induced lower updrafts and WP (Figure 11a). This comparison between the ice and noice runs confirms that the presence of ice processes and the associated WBF mechanism plays a critical role in the lower aerosol-induced increases in condensation than in evaporation in the ice runs. Figure 13 schematically depicts the flow of processes that are described in Section 4.2.1.

4.2.2 INP

Deleted: 9

Deleted: 9

Deleted: 9

Deleted: 1

So far, we have examined effects of the increasing concentration of aerosols acting as CCN. However, unlike situations in warm stratocumulus clouds that have garnered most of attention in terms of aerosol-cloud interactions, not only aerosols acting as CCN but also those acting as INP can affect mixed-phase stratocumulus clouds (Rangno and Hobbs, 2001; Lohmann, 2002; Borys et al., 2003). The above-described INP-10 and INP-100 runs as compared to the control run identifies how the increasing concentration of aerosols acting as INP affects mixed-phase clouds. As seen in this comparison, the increasing concentration of aerosols acting as INP causes WP to increase, contrary to effects of the increasing concentration of aerosols acting as CCN. However, at each time step and grid point, a factor by which the concentration of background aerosols acting as CCN varies between the control and low-aerosol runs is different from that by which the concentration of background aerosols acting as INP varies among the control, INP-10 and INP-100 runs. For better comparisons between CCN and INP effects, it is better to make consistency in the factors between simulations for CCN effects and those for INP effects. For this consistency, the INP-reduced run is performed as the repeated control run by reducing the concentration of background aerosols acting as INP (but not CCN) at each time step and grid point by the same factor as used for the reduction in the concentration of background aerosols acting as CCN in the low-aerosol run as compared to that in the control run. The INP-reduced run is compared to the control run to examine the INP effects. The INP-reduced run is identical to the low-aerosol run except that the concentration of background aerosols acting as INP but not CCN at every time step and grid point after 05:00 LST on January 12th is assumed to have that at 05:00 LST on January 12th.

Figure 11d shows the time series of differences in deposition rate, condensation rate and related variables between the control and INP-reduced runs. With the increasing concentration of background aerosols acting as INP, there are more increases in CINC between those runs than between the control and low-aerosol runs (Figures 11a and 11d). During the initial stage before 20:00 LST on January 12th, overall, there is an increasing temporal trend in differences in CINC between the control and INP-reduced runs due to the larger increasing temporal trend in CINC in the control run than in the INP-reduced run (Figure 11d). Increasing CINC provides the increasing integrated surface area of ice crystals for deposition. This leads to the increasing temporal trend in deposition, which is

larger in the control run, and in differences in deposition between the control and INP-reduced runs (Figure 11d). However, due to no changes in the concentration of the background aerosols acting as CCN between the control and INP-reduced runs, there are negligible differences in CDNC between the control and INP-reduced runs as compared to those between the control and low-aerosol runs (Figures 11a and 11d). More evaporation occurs in the control run than in the INP-reduced run and this is contributed by the more deposition and associated WBF mechanism (Figure 11d). Also, more entrainment contributes to the more evaporation in the control run (Figure 11b). Between the INP-reduced and control runs, with no increases in the concentration of background aerosols acting as CCN, increases in the surface-to-volume ratio of droplets and the associated enhancement in the WBF-mechanism-related efficiency of evaporation are negligible as compared to those between the control and low-aerosol runs. Note that there are overall larger increases in entrainment and associated evaporation between the control and INP-reduced runs than between the control and low-aerosol runs (Figure 11b). The negligible enhancement in the WBF-mechanism-related efficiency of evaporation overshadows the overall larger increases in entrainment and associated evaporation between the control and INP-reduced runs. This leads to aerosol-induced overall smaller increases in evaporation between the control and INP-reduced runs than between the control and low-aerosol runs (Figures 11a and 11d).

Mainly due to the increase in evaporation, there is more negative buoyancy and updraft mass fluxes start to reduce in the control run as compared to those in the INP-reduced run around 12:50 LST on January 12th (Figure 11d). Eventually, updraft mass fluxes in the control run become smaller than those in the INP-reduced run around 15:50 LST on January 12th (Figure 11d). This decrease occurs to a lesser extent mainly due to overall smaller aerosol-induced increases in evaporation between the control and INP-reduced runs than between the control and low-aerosol runs (Figures 11a and 11d). Associated with weaker updrafts in the control run, condensation in the control run becomes smaller than that in the INP-reduced run around 15:50 LST on January 12th but to a lesser degree as compared to that between the control and low-aerosol runs (Figures 11a and 11d).

Deleted: 9

Deleted: 9
Deleted: 9

Deleted: 9
Deleted: 9

Deleted: 9

Deleted: 9
Deleted: 9

Deleted: 9

Deleted: 9

Deleted: 9
Deleted: 9

Deleted: 9
Deleted: 9

1305   When there is aerosol-induced reduction in condensation, there starts to be more

1306   available water vapor for deposition and thus aerosol-induced increases in deposition

1307   between the control and INP-reduced runs jump around 15:50 LST on January 12th (Figure

1308   11d). This is similar to the situation between the control and low-aerosol runs. However,

1309   due to greater aerosol-induced increases in CINC and the associated integrated surface area

1310   of ice crystals, after ~ 15:50 LST on January 12th, there are greater aerosol-induced

1311   increases in deposition between the control and INP-reduced runs than between the control

1312   and low-aerosol runs (Figures 11a and 11d). Remember that the decrease in condensation,

1313   starting around 15:50 LST on January 12th, between the control and INP-reduced runs is

1314   smaller than that between the control and low-aerosol runs. This enables the increase in

1315   deposition to overcome the decrease in condensation between the control and INP-reduced

1316   runs. The larger increase in deposition than the decrease in condensation between the

1317   control and INP-reduced runs eventually makes updrafts in the control run greater than

1318   those in the INP-reduced run around 18:50 LST on January 12th (Figure 11d).

1319   Initiated by aerosol-induced greater increase in deposition during the initial stage,

1320   there is aerosol-induced greater increase in IWP between the control and INP-reduced runs

1321   than between the control and low-aerosol runs over the whole simulation period (Figure

1322   14). Initiated by aerosol-induced smaller decrease in condensation during the initial stage,

1323   there is aerosol-induced smaller decrease in LWP between the control and INP-reduced

1324   runs than between the control and low-aerosol runs over the whole simulation period

1325   (Figure 14). This greater increase in IWP dominates over the smaller decrease in LWP

1326   between the control and INP-reduced runs, leading to an increase in WP in the control run

1327   as compared to that in the INP-reduced run with an increase in the average cloud fraction

1328   over time steps with non-zero cloud fraction from 0.89 in the INP-reduced run to 0.92 in

1329   the control run. This is in contrast to the situation between the control and low-aerosol runs.

1330   Hence, comparisons between the control, INP-reduced and the low-aerosol runs

1331   demonstrate that whether there is an increasing concentration of aerosols acting as INP or

1332   CCN has substantial impacts on how WP responds to the increasing concentration of

1333   aerosols.

1334

1335   **4.2.3   Sedimentation of ice particles**

Deleted: 9

Deleted: 9

Deleted: 9

Deleted: 9

Deleted: 2

Deleted: 2

1342

1343   With increasing concentrations of aerosols acting as CCN between the control and low-

1344   aerosol runs, the size and fall velocity of ice crystals do not change significantly at the

1345   initial stage. The average ice-crystal radius over grid points and time steps with non-zero

1346   CINC for the initial stage is 54 and 52 μm in the control and low-aerosol runs, respectively.

1347   This means that aerosol-induced changes in the sedimentation of ice crystals do not affect

1348   CINC, the associated integrated surface area of ice crystals and deposition significantly.

1349   Moreover, as described in Section 4.2.1, the CDNC evolution (but not the CINC evolution)

1350   plays a critical role in the different evolution of evaporation, condensation, and deposition

1351   at the initial stage between the runs. Hence, it is not likely that aerosol-induced changes in

1352   the sedimentation of ice crystals and associated ice particles such as snow, and associated

1353   CINC have a significant impact on aerosol-induced changes in those phase-transition

1354   processes at the initial stage and subsequently at later stages. To check this out, the control

1355   and low-aerosol runs are repeated by setting the fall velocity of ice particles (including ice

1356   crystals) to zero. These repeated runs are the control-no-sedim and low-aerosol-no-sedim

1357   runs. Hence, in these repeated runs, there are no aerosol-induced changes in the

1358   sedimentation of ice particles. The time- and domain-averaged IWP, LWP and WP are 14

1359   (12), 5 (8) and 19 (20) g m^{-2}, respectively, in the control-no-sedim (low-aerosol-no-sedim)

1360   run. The time- and domain-averaged IWP, LWP and WP are 11 (10), 7 (9), 18 (19) g m^{-2},

1361   respectively, in the control (low-aerosol) run. The presence of the sedimentation decreases

1362   IWP and increases LWP as compared to the situation with no sedimentation for each of the

1363   control and low-aerosol runs. The differences in IWP and LWP between the control-no-

1364   sedim and low-aerosol-no-sedim runs is slightly greater than that between the control and

1365   low-aerosol runs. Hence, the presence of impacts of aerosols acting as CCN on the

1366   sedimentation reduces aerosol impacts on IWP and LWP. However, results here show that

1367   the qualitative nature of impacts of aerosols acting as CCN on cloud mass does not vary,

1368   whether there are changes in the sedimentation of ice particles with increasing

1369   concentrations of aerosols acting as CCN. This indicates that the presence of the

1370   sedimentation and its aerosol-induced changes is not a factor that controls the qualitative

1371   nature of impacts of aerosols acting as CCN on cloud mass.

1372   With increasing concentrations of aerosols acting as INP between the control and INP-

1373   reduced runs, the size and fall velocity of ice crystals change at the initial stage. The

1374   average ice-crystal radius over grid points and time steps with non-zero CINC for the initial

1375   stage is 54 and 59 μm in the control and INP-reduced runs, respectively. To see the effect

1376   of these changes in the size and associated sedimentation of ice particles on the qualitative

1377   nature of results between the control and INP-reduced runs, the INP-reduced run is

1378   repeated by setting the fall velocity of ice particles to zero. This repeated run is referred to

1379   as the INP-reduced-no-sedim run. The time- and domain-averaged IWP, LWP and WP are

1380   14 (11), 5 (6) and 19 (17) g m^{-2}, respectively, in the control-no-sedim (INP-reduced-no-

1381   sedim) run, while the time- and domain-averaged IWP, LWP and WP are 11 (7), 7 (8) and

1382   18 (15) g m^{-2}, respectively, in the control (INP-reduced) run. The presence of the

1383   sedimentation decreases IWP and increases LWP as compared to the situation with no

1384   sedimentation for each of the control and INP-reduced runs. The difference in IWP

1385   between the control-no-sedim and INP-reduced-no-sedim runs is smaller than that between

1386   the control and INP-reduced runs. The difference in LWP between the control-no-sedim

1387   and INP-reduced-no-sedim runs is not different from that between the control and INP-

1388   reduced runs. Hence, the presence of impacts of aerosols acting as INP on the

1389   sedimentation enhances aerosol impacts on IWP, although the presence does not affect

1390   aerosol impacts on LWP. However, the qualitative nature of impacts of aerosols acting as

1391   INP on cloud mass also does not vary, whether there are changes in the sedimentation of

1392   ice particles with increasing concentrations of aerosols acting as INP. This indicates that

1393   the presence of the sedimentation and its aerosol-induced changes is not a factor that

1394   controls the qualitative nature of impacts of aerosols acting as INP on cloud mass.

1395

1396   **5. Summary and conclusions**

1397

1398 When it comes to stratocumulus clouds and their interactions with aerosols, warm clouds,

1399 which are composed of liquid particles only, have garnered most of the attention. However,

1400 in mid-latitudes, particularly during the wintertime, there are frequent occurrences of

1401 mixed-phase stratocumulus clouds, which are composed of both liquid and solid particles.

1402 The level of understanding of mechanisms that control the development of these mixed-

1403 phase clouds and their interactions with aerosols has been low. Motivated by this, this study
1404 aims to improve our understanding of the development of these mixed-phase stratocumulus
1405 clouds and their interactions with aerosols by focusing on roles of ice particles and
1406 processes in the development and interactions.

1407 Ice crystals (i.e., cloud ice) and their interactions with droplets (i.e., cloud liquid) in a
1408 selected system of mixed-phase stratocumulus clouds lower cloud mass substantially as
1409 compared to that in warm stratocumulus clouds. This is due to insufficient compensation
1410 of the reduced condensation and LWP by deposition and IWP in the mixed-phase clouds.
1411 This insufficient compensation is related to low CINC and associated low integrated
1412 surface area of ice crystals in the mixed-phase clouds. As the concentration of aerosols
1413 acting as INP and CINC increase, deposition enhances and this enables cloud mass in the
1414 mixed-phase clouds to be similar to that in the warm clouds.

1415 In the mixed-phase clouds, with the increasing concentration of aerosols acting as
1416 CCN, there are decreases in cloud mass. In the mixed-phase clouds, aerosol-induced
1417 increases in the evaporation of droplets, which involve the WBF mechanism, and their
1418 impacts on updrafts outweigh aerosol-intensified feedbacks between condensation and
1419 updrafts. This leads to aerosol-induced decreases in cloud mass. However, in the warm
1420 clouds, with the increasing concentration of aerosols acting as CCN, there are increases in
1421 cloud mass. Due to the absence of the WBF mechanism, in the warm clouds, aerosol-
1422 induced increases in the evaporation of droplets are not as efficient as in the mixed-phase
1423 clouds. This enables aerosol-intensified feedbacks between condensation and updrafts to
1424 induce aerosol-induced increases in cloud mass in the warm clouds. With the increases in
1425 the concentration of aerosols acting as INP, there are aerosol-induced greater increases in
1426 CINC and deposition than with the increases in the concentration of aerosols acting as
1427 CCN. This enables the increasing concentration of aerosols acting as INP to induce
1428 increases in cloud mass, which is in contrast to the situation with the increasing
1429 concentration of aerosols acting as CCN.

1430 It is generally true that the conventional wisdom of stratiform clouds and aerosol
1431 effects on them has been established mostly by relying on warm clouds (Ramaswamy et
1432 al., 2001; Forster et al., 2007; Wood, 2012). For example, this wisdom generally indicates
1433 that increasing concentrations of aerosols acting as CCN increase cloud mass (Albrecht,

1989). However, in contrast to this, this study shows that in the mixed-phase stratiform clouds, the increasing concentration of aerosols acting as CCN can reduce cloud mass via CCN-induced changes in interactions between ice and liquid particles. It is also shown that the increasing concentration of aerosols acting as INP enhances cloud mass via INP-induced changes in interactions between ice and liquid particles, in contrast to roles of the increasing concentration of aerosols acting as CCN in cloud mass. In addition, this study finds that the presence of ice particles and its interactions with liquid particles reduce cloud mass in the mixed-phase clouds as compared to that in warm clouds. Mid-latitude winter stratiform clouds and high-latitude clouds such as the Arctic stratiform clouds frequently involve ice particles as well as liquid particles. As discussed in Stevens and Feingold (2009), our lack of understanding of these clouds and their interactions with aerosols has made a significant contribution to the high uncertainty in the prediction of climate change. Hence, to reduce this uncertainty especially by reducing the related uncertainty in climate models, we have to go beyond the warm-cloud-based traditional parameterizations of clouds and their interactions with aerosols in climate models. For this, this study indicates that it is imperative to develop new parameterizations that consider impacts of interactions between ice and liquid particles on clouds, and the interplay of those impacts with varying concentrations of aerosols acting not only as CCN but also as INP.

The average CINC in the control run in this study is on the order of magnitude of ~0.1 cm^{-3} and this is an order of magnitude lower than that in the control run in Lohmann and Diehl (2006) for similar temperature and CDNC ranges between the runs. Remember that this study uses parameterizations by Lohmann and Diehl (2006) for the heterogeneous INP activation. In the control run in Lohmann and Diehl (2006), the INP concentrations, which are dependent only on temperature, are used for the INP activation. However, in the control run in this study, instead of obtaining the INP concentrations empirically using the temperature as in Lohmann and Diehl (2006), the observed spatiotemporal variation of the INP concentration is considered for the INP activation. Lohmann and Diehl (2006) have shown that using the INP concentrations, which are empirically obtained based only on temperature, for the INP activation can increase CINC by a factor of ~10 as compared to that when the spatiotemporal variation of the INP concentration, as a result of above-mentioned processes related to aerosols, is considered for the activation. It is believed that

this explains the discrepancy in CINC between the control in this study and that in Lohmann and Diehl (2006).

Note that many of the previous studies of mixed-phase stratocumulus clouds (e.g., Ovchinnikov et al., 2011; Possner et al., 2017) have focused on roles of cloud-top radiative cooling, entrainment and sedimentation of ice particles in mixed-phase stratocumulus clouds and their interactions with aerosols. However, there have not been many studies that focus on roles of microphysical interactions, which involve microphysical processes (e.g., evaporation, condensation and deposition) and factors (e.g., cloud-particle concentrations and sizes), between ice and liquid particles in those clouds and their interplay with aerosols. Hence, we believe that this study contributes to the more general understanding of mixed-phase clouds and their interactions with aerosols.

Code/Data availability

The Code/data used are currently private and stored in our private computer system. Opening the data to the public requires approval from funding sources. Since funding projects associated with this work are still going on, these sources do not allow the data to be open to the public; 2–3 years after these project ends, the data can be open to the public. However, if there is any inquiry about the data, contact the corresponding author Seoung Soo Lee (slee1247@umd.edu).

Author contributions

SSL and KJH established essential initiative ideas to start this work. While SSL worked on the analysis of simulation data, KJH and MGM worked on the analysis of observation data. MK, HK, NU, and JG participated in the preliminary analysis of simulation and observation data, and provided ideas to improve the presentation of results by reviewing the manuscript. YZ, KOC and GUK provided ideas to deal with reviewers' comments, while CHJ and JU performed additional simulations and associated analysis to handle those comments.

Competing interests

The authors declare that they have no conflict of interest.

Acknowledgements

This study is supported by the National Research Foundation of Korea (NRF) grant funded by the Korea government (MSIT) (No. NRF2020R1A2C1003215) and the "Construction of Ocean Research Stations and their Application Studies" project, funded by the Ministry of Oceans and Fisheries, South Korea

References

Ackerman, A. S., Kirkpatrick, M. P., Stevens, D. E., and Toon, O. B.: The impact of humidity above stratiform clouds on indirect aerosol climate forcing, Nature, 432, 1014-1017, 2004.

Albrecht, B. A.: Aerosols, cloud microphysics, and fractional cloudiness, Science, 245, 1227-1230, 1989.

Bergeron, T.: On the physics of clouds and precipitation. Proces Verbaux de l'Association de Meteorologie, International Union of Geodesy and Geophysics, 156–178, 1935.

Bodas-Salcedo, A., Hill, P. G., Furtado, K., Williams, K. D., Field, P. R., Manners, J. C., Hyder, P., and Kato, S.: Large contribution of supercooled liquid clouds to the solar radiation budget of the Southern Ocean, J. Climate, 29, 4213–4228, doi:10.1175/JCLI-D-15-0564.1, 2016.

Borys, R. D., Lowenthal, D. H., Cohn, S. A. and Brown, W. O. J.: Mountaintop and radar measurements of anthropogenic aerosol effects on snow growth and snowfall rate. Geophys. Res. Lett., 30, 1538, doi:10.1029/2002GL016855 ,2003.

Brown, A., Milton, S., Cullen, M., Golding, B., Mitchell, J., and Shelly, A.: Unified modeling and prediction of weather and climate: A 25-year journey, Bull. Am Meteorol. Soc. 93, 1865–1877, 2012.

Chen, F., and Dudhia, J.: Coupling an advanced land-surface hydrology model with the Penn State-NCAR MM5 modeling system. Part I: Model description and implementation, Mon. Wea. Rev., 129, 569–585, 2001.

Dong, X., and Mace, G. G.: Arctic stratus cloud properties and radiative forcing derived from ground-based data collected at Barrow, Alaska. J. Climate, 16, 445–461, doi:10.1175/1520-0442(2003)016,0445:ASCPAR.2.0.CO;2, 2003.

Eun, S.-H., Kim, B.-G., Lee, K.-M., and Park, J.-S.: Characteristics of recent severe haze events in Korea and possible inadvertent weather modification, SOLA, 12, 32-36, 2016.

Faller, K: MTSAT-1R: A multifunctional satellite for Japan and the Asia-Pacific region, Proceedings of the 56th IAC 2005, Fukuoda, Japan, Oct. 17-21, 2005, IAC-05-B3.2.04

1560 Fan, J., Yuan, T., Comstock, J. M., et al.: Dominant role by vertical wind shear in regulating
1561   aerosol effects on deep convective clouds, J. Geophys. Res., 114,
1562   doi:10.1029/2009JD012352, 2009.

1563 Findeisen, W.: Kolloid-meteorologische Vorgange bei Neiderschlagsbildung. Meteor. Z.,
1564   55, 121–133, 1938.

1565 Forster, P., et al., Changes in atmospheric constituents and in radiative forcing, in: Climate
1566   change 2007: the physical science basis, Contribution of working group I to the Fourth
1567   Assessment Report of the Intergovernmental Panel on Climate Change, edited by
1568   Solomon, S., et al., Cambridge Univ. Press, New York, 2007.

1569 Fouquart, Y., and Bonnel, B.: Computation of solar heating of the Earth's atmosphere: a
1570   new parameterization, Beitr. Phys. Atmos., 53, 35-62, 1980.

1571 Grell, G. A., Peckham, S. E., Schmitz, R., McKeen, S. A., Frost, G., Skamarock, W. C.,
1572   and Eder, B.: Fully coupled online chemistry in the WRF model, Atmos.
1573   Environ., 39, 6957– 6976, 2005.

1574 Guo, J., M. Deng, S. S. Lee, F. Wang, Z. Li, P. Zhai, H. Liu, W. Lv, W. Yao, and X. Li:
1575   Delaying precipitation and lightning by air pollution over the Pearl River Delta. Part
1576   I: Observational analyses, J. Geophys. Res. Atmos., 121, 6472–6488,
1577   doi:10.1002/2015JD023257, 2016.

1578 Ha, K.-J., Nam, S., Jeong, J.-Y., et al., Observations utilizing Korean ocean research
1579   stations and their applications for process studies, Bull. Amer. Meteor. Soc., 100,
1580   2061-2075, 2019.

1581 Hahn, C. J., and Warren, S. G.: A gridded climatology of clouds over land (1971–96) and
1582   ocean (1954–97) from surface observations worldwide. Numeric Data Package NDP-
1583   026EORNL/CDIAC-153, CDIAC, Department of Energy, Oak Ridge, TN, 2007.

1584 Hartmann, D. L., Ockert-Bell, M. E., and Michelsen, M. L.: The effect of cloud type on
1585   earth's energy balance—Global analysis, J. Climate, 5, 1281–1304, 1992.

1586 Holben, B. N., Tanré, D., Smirnov, et al.: An emerging ground-based aerosol climatology:
1587   Aerosol optical depth from AERONET, J. Geophys. Res., 106, 12067–12097, 2001.

1588 Hu, Y., Rodier, S., Xu, K.-M., Sun, W., Huang, J., Lin, B., Zhai, P., and Josset, D.:
1589   Occurrence, liquid water content and fraction of supercooled water clouds from
1590   combined CALIOP/IIR/MODIS measurements, J. Geophys. Res., 115, D00H34,

1591   doi:10.1029/2009JD012384, 2010.

1592   Huang, Y., Siems, S. T., Manton, M. J., Protat, A. and Delanöe, J.: A study on the low-
1593   altitude clouds over the Southern Ocean using the DARDAR-MASK, J. Geophys.
1594   Res., 117, D18204, doi:10.1029/2012JB009424, 2012.

1595   Intrieri, J. M., Shupe, M. D., Uttal, T. and McCarty, B. J.: An annual cycle of Arctic cloud
1596   characteristics observed by radar and lidar at SHEBA, J. Geophys. Res., 107, 8030,
1597   doi:10.1029/2000jc000423, 2002.

1598   Jackson, R. C., and Coauthors: The dependence of Arctic mixed-phase stratus ice cloud
1599   microphysics on aerosol concentration using observations acquired during ISDAC
1600   and M-PACE, J. Geophys. Res., 117, D15207, doi:10.1029/2012JD017668, 2012.

1601   Kanitz, T., Seifert, P., Ansmann, A., Engelmann, R., Althausen, D., Casiccia, C. and
1602   Rohwer, E. G.: Contrasting the impact of aerosols at northern and southern
1603   midlatitudes on heterogeneous ice formation, Geophys. Res. Lett., 38,
1604   L17802,doi:10.1029/2011GL048532, 2011.

1605   Khain, A., BenMoshe, N. and Pokrovsky, A.: Factors determining the impact of aerosols
1606   on surface precipitation from clouds: Attempt of classification, J. Atmos. Sci., 65,
1607   1721 – 1748, 2008.

1608   Khain, A., Pokrovsky, A., Rosenfeld, D., Blahak, U., and Ryzhkoy, A.: The role of CCN in
1609   precipitation and hail in a mid-latitude storm as seen in simulations using a spectral
1610   (bin) microphysics model in a 2D dynamic frame, Atmos. Res., 99, 129–146, 2011.

1611   Klemp, J. B., Skamarock, W. C., and Dudhia, J.: Conservative split-explicit time
1612   integration methods for the compressible nonhydrostatic equations, Mon. Weather
1613   Rev., 135, 2897 – 2913, 2007.

1614   Koop, T., Luo, B. P., Tsias, A. and Peter, T.: Water activity as the determinant for
1615   homogeneous ice nucleation in aqueous solutions, Nature, 406, 611-614, 2000.

1616   Lance, S., Brock, C. A., Rogers, D. and Gordon, J. A.: Water droplet calibration of the
1617   Cloud Droplet Probe (CDP) and inflight performance in liquid, ice and mixed-phase
1618   clouds during ARCPAC, Atmos. Meas. Tech., 3, 1683–1706, doi:10.5194/amt-3-
1619   1683-2010, 2010.

1620   Lebo, Z. J., and Morrison, H.: Dynamical effects of aerosol perturbations on simulated
1621   idealized squall lines, Mon. Wea. Rev., 142, 991-1009, 2014.

1622   Lee, S., Ho, C.-H., Lee, Y. G., Choi, H.-J. and Song, C.-K.: Influence of transboundary air
1623   pollutants from China on the high-PM10 episode in Seoul, Korea for the period
1624   October 16−20, 2008. Atmos. Environ., 77, 430−439, 2013.

1625   Lee, S. S., Kim, B.-G., and Yum, S. S., et al.: Effect of aerosol on evaporation, freezing and
1626   precipitation in a multiple cloud system, Clim. Dyn., 48, 1069-1087, 2016.

1627   Lee, S. S., Donner, L. J., Phillips, V. T. J. and Ming, Y.: The dependence of aerosol effects
1628   on clouds and precipitation on cloud-system organization, shear and stability. J.
1629   Geophys. Res., 113, D16202, doi:10.1029/2007JD009224, 2008.

1630   Lohmann, U.:Aglaciation indirect aerosol effect caused by soot aerosols, Geophys. Res.
1631   Lett., 29, doi:10.1029/2001GL014357, 2002.

1632   Michalakes, J., Chen, S., Dudhia, J., Hart, L., Klemp, J., Middlecoff, J. and Skamarock,
1633   W.: Development of a next generation regional weather research and forecast model,
1634   in Developments in Teracomputing: Proceedings of the Ninth ECMWF Workshop on
1635   the Use of High Performance Computing in Meteorology, edited by W. Zwieflhofer
1636   and N. Kreitz, pp. 269 – 276, World Sci., Singapore, 2001.

1637   Mlawer, E. J., Taubman, S. J., Brown, P. D., Iacono, M. J., and Clough, S. A.: RRTM, a
1638   validated correlated-k model for the longwave, J. Geophys. Res., 102, 16663-1668,
1639   1997.

1640   Morrison, A. E., Siems, S. T. and Manton, M. J.: A three year climatology of cloud-top
1641   phase over the Southern Ocean and North Pacific, J. Climate, 24, 2405–
1642   2418,doi:10.1175/2010JCLI3842.1, 2011.

1643   Morrison, H., and Grabowski, W. W.: Cloud-system resolving model simulations of aerosol
1644   indirect effects on tropical deep convection and its thermodynamic environment,
1645   Atmos. Chem. Phys., 11, 10503–10523, 2011.

1646   Möhler, O., et al, Efficiency of the deposition mode ice nucleation on mineral dust particles,
1647   Atmos. Chem. Phys., 6, 3007-3021, 2006.

1648   Naud, C., Booth, J. F. and Del Genio, A. D.: Evaluation of ERA-Interim andMERRA
1649   cloudiness in the Southern Ocean, J. Climate, 27, 2109–2124, doi:10.1175/JCLI-D-
1650   13-00432.1, 2014.

1651   Oh, H.-R., Ho, C.-H., Kim, J., Chen, D., Lee, S., Choi, Y.-S., Chang, L.-S., and Song, C.-
1652   K.: Long-range transport of air pollutants originating in China: A possible major cause

of multi-day high-PM10 episodes during cold season in Seoul, Korea. Atmos. Environ., 109, 23−30, 2015.

Ovchinnikov, M., Korolev, A., and Fan, J.: Effects of ice number concentration on dynamics of a shallow mixed-phase stratiform cloud, J. Geophys. Res., 116, D00T06, doi:10.1029/2011JD015888, 2011.

Possner, A., Ekman, A. M. L., and Lohmann, U.: Cloud response and feedback processes in stratiform mixed-phase clouds perturbed by ship exhaust, Geophys. Res. Lett., 44, 1964–1972, doi:10.1002/2016GL071358, 2017.

Pruppacher, H. R. and Klett, J. D.: Microphysics of clouds and precipitation, 714pp, D. Reidel, 1978.

Rangno, A. L., and Hobbs, P. V.: Ice particles in stratiform clouds in the Arctic and possible mechanisms for the production of high ice concentrations, J. Geophys. Res., 106,15 065–15 075, doi:10.1029/2000JD900286, 2001.

Ramaswamy, V., et al.: Radiative forcing of climate change, in Climate Change 2001: The Scientific Basis, edited by J. T. Houghton et al., 349-416, Cambridge Univ. Press, New York, 2001.

Shupe, M. D., Uttal, T., Matrosov, S, Y. and Rrisch, A. S.: Cloud water contents and hydrometeor sizes during the FIRE Arctic clouds experiment, J. Geophys. Res., 106, 15 015–15 028, doi:10.1029/2000JD900476, 2001.

Shupe, M. D., Uttal, T. and Matrosov, S. Y.: Arctic cloud microphysics retrievals from surface-based remote sensors at SHEBA, J. Appl. Meteor., 44, 1544–1562, doi:10.1175/JAM2297.1, 2005.

Skamarock, W. C., Klemp, J. B., Dudhia, J., Gill, D. O., Barker, D. M., Duda, M. G., Wang, W., and Powers, J. G.: A description of the advanced research WRF version 3, NCAR Tech. Note NCAR/TN-475+STR, 113 pp., Boulder, Colo., 2008.

Stephens, G. L., and Greenwald, T. J.: Observations of the Earth's radiation budget in relation to atmospheric hydrology. Part II: Cloud effects and cloud feedback. J. Geophys. Res., 96, 15 325–15 340, 1991.

Stevens, B., and Feingold, G.: Untangling aerosol effects on clouds and precipitation in a buffered system, Nature, 461, 607-613, 2009.

Twomey, S.: The influence of pollution on the shortwave albedo of clouds, J. Atmos. Sci.,

1684   34, 1149-1152, 1977.

1685 Twomey, S.: Pollution and the Planetary Albedo, Atmos. Env., 8,1251-1256, 1974.

1686 Wang, H., Skamarock, W. C., and Feingold, G.: Evaluation of scalar advection schemes in
1687   the Advanced Research WRF model using large-eddy simulations of aerosol-cloud
1688   interactions, Mon. Wea. Rev., 137, 2547-2558, 2009.

1689 Warren, S. G., Hahn, C. J., London, J., Chervin, R. M., and Jenne, R. L.: Global distribution
1690   of total cloud cover and cloud types over land. NCAR Tech. Note NCAR/TN-
1691   273+STR, National Center for Atmospheric Research, Boulder, CO, 29 pp. + 200
1692   maps, 1986.

1693 Wegener, A.: Thermodynamik der Atmosphare. J. A. Barth, 311 pp, 1911.

1694 Wood, R.: Stratocumulus clouds, Mon. Wea. Rev., 140, 2373-2423, 2012.

1695 Young, G., Connolly, P. J., Jones, H. M., and Choularton, T. W.: Microphysical sensitivity
1696   of coupled springtime Arctic stratocumulus to modelled primary ice over the ice pack,
1697   marginal ice, and ocean, Atmos. Chem. Phys., 17, 4209–4227,
1698   https://doi.org/10.5194/acp-17-4209-2017, 2017.

1699 Zuidema, P., Westwater, E. R., Fairall, C. and Hazen, D.: Ship-based liquid water path
1700   estimates in marine stratocumulus, J. Geophys. Res., 110, D20206,
1701   doi:10.1029/2005JD005833, 2005.

1702
1703
1704
1705
1706
1707
1708
1709
1710
1711
1712
1713
1714
1715
1716
1717
1718
1719
1720

FIGURE CAPTIONS

Figure 1. A rectangle represents the domain of interest in terms of the aerosol advection. A dot on the top-right corner of the rectangle marks a station that measures PM_{10} and $PM_{2.5}$ in Baekryongdo island as detailed in Section 2. An area to the east of the yellow line in the rectangle is the Seoul area. In the Seoul area, a dot marks a representative station that measures PM_{10} and $PM_{2.5}$ in the Seoul area as detailed in Section 2. A closed dotted line marks the boundary of the Seoul city.

Figure 2. (a) Time series of PM_{10} and $PM_{2.5}$ observed at the ground station in Baekryongdo island (BN) and a representative ground station in the Seoul area (SL). The abscissa represents days between January 10th and 19th in 2013. The blue (red) arrow marks time when aerosol mass starts to increase in BN (SL) due to the advection of aerosols from East Asia to the Seoul area. The spatial distribution of $PM_{2.5}$, which is observed and measured by the ground stations and interpolated into grid point over the rectangle in Figure 1, at (b) 05:00 LST and (c) 18:00 LST on January 12th in 2013.

Figure 3. The vertical distributions of the radiosonde-observed (a) potential temperature and (b) water-vapor mass density at 03:00 LST and 15:00 LST on January 12th.

Figure 4. Aerosol size distribution at the surface. N represents aerosol number concentration per unit volume of air and D represents aerosol diameter.

Figure 5. Time series of (a) the domain-averaged liquid-water path (LWP), ice-water path (IWP) and water path (WP), which is the sum of LWP and IWP, for the control run, and LWP for the control-noice run, and (b) the domain-averaged condensation rates, deposition rates and the sum of those rates in the control run and condensation rates in the control-noice run. (c) Vertical distribution of the time- and domain-averaged evaporation rates and (d) the average CDNC over grid points and time steps with non-zero CDNC for the initial stage between 00:00 LST and 20:00 LST on January 12th.

1756   Figure 6. Vertical distributions of (a) the time- and domain-averaged updraft mass fluxes

1757   for the control and control-noice runs and (b) the average cloud ice number concentration

1758   (CINC) over grid points and time steps with non-zero CINC (for the whole domain and

1759   simulation period in the control run).

1760

1761   Figure 7. Cumulative frequency of (a) WP in the control run and LWP, which is WP, in

1762   the control-noice run and (b) LWP and IWP in the control run and LWP in the control-

1763   noice run at the last time step.

1764

1765   Figure 8. (a) Vertical distributions of the average CINC over grid points and time steps

1766   with non-zero CINC (for the whole domain and simulation period) in the control, INP-10,

1767   and INP-100 runs. Time series of the domain-averaged condensation rates, deposition rates

1768   and the sum of those rates (b) in the INP-10 run and (c) in the INP-100 run. In (b) and (c),

1769   condensation rates in the control-noice run are additionally displayed.

1770

1771   Figure 9. (a) Time series of the domain-averaged LWP, IWP and WP for the control run,

1772   LWP for the control-noice run and WP for the INP-10 and INP-100 runs. (b) Cumulative

1773   frequency of LWP, IWP and WP for the control, INP-10 and INP-100 runs at the last time

1774   step.

1775

1776   Figure 10. (a) Time series of the domain-averaged LWP, IWP and WP for the control and

1777   low-aerosol runs, and LWP, which is also WP, for the control-noice and low-aerosol-noice

1778   runs. (b) Cumulative frequency of WP for the control, low-aerosol run, control-noice and

1779   low-aerosol-noice runs, and (c) LWP and IWP for the control and low-aerosol runs and

1780   LWP in the control-noice and low-aerosol-noice runs at the last time step.

1781

1782   Figure 11. (a) Time series of differences in the domain-averaged updraft mass fluxes,

1783   deposition, condensation and evaporation rates, the average CDNC (CINC) over grid

1784   points with non-zero CDNC (CINC) between the control and low-aerosol runs (the control

1785   run minus the low-aerosol run). (b) Time series of differences in the average entrainment

1786   rate over all grid points at the PBL tops between the control and low-aerosol runs (the

control run minus the low-aerosol run) and between the control and INP-reduced runs (the control run minus the INP-reduced run). (c) Same as (a) but between the control-noice and low-aerosol-noice runs (the control-noice run minus the low-aerosol-noice run) and (d) same as (a) but between the control and INP-reduced runs (the control run minus the INP-reduced run). Dashed lines in (a), (b), (c) and (d) represent zero differences. In (c), due to the absence of ice processes in the noice runs, differences in deposition rates and CINC are absent. A green-dashed box in (a) and (b) marks a time period when steady and rapid temporal increases in the CDNC differences and a jump in differences in each of condensation and evaporation rates between the control and low-aerosol runs occur (see text for details).

Figure 12. Vertical distributions of the average CDNC over grid points and time steps with non-zero CDNC (for the whole domain and simulation period) (a) in the control and low-aerosol runs, and (b) in the control-noice and low-aerosol-noice runs.

Figure 13. A schematic diagram that depicts the flow of processes that are described in Section 4.2.1 and associated with responses of clouds to increasing aerosols acting as CCN.

Figure 14. Time series of the domain-averaged LWP, IWP and WP for the control, low-aerosol and INP-reduced runs, and LWP, which is also WP, for the control-noice and low-aerosol-noice runs.

Simulations	Increases in the background concentration of aerosols acting as CCN due to the aerosol advection after 05:00 LST on January 12th	Ice processes	Background concentration of aerosols acting as INP	Ice-particle Sedimentation	Liquid-particle Sedimentation
Control run	Present	Present	100 times lower than the background concentration of aerosols acting as CCN	Present	Present
Low-aerosol run	Absent	Present	Same as in the control run	Present	Present
Control-noice run	Present	Absent	Absent	Present	Present
Low-aerosol-noice run	Absent	Absent	Absent	Present	Present
INP-10 run	Present	Present	10 times higher than in the control run	Present	Present
INP-100 run	Present	Present	100 times higher than in the control run	Present	Present
INP-reduced run	Present	Present	Reduced in the same way as CCN is reduced in the low-aerosol run	Present	Present
Control-no-sedim	Present	Present	Same as in the control run	Absent	Present

Formatted Table

Control-no-sedim-ice-liq	Present	Present	Same as in the control run	Absent	Absent
Low-aerosol-no-sedim	Absent	Present	Same as in the control run	Absent	Present
INP-10-no-sedim	Present	Present	Same as in the INP-10 run	Absent	Present
INP-100-no-sedim	Present	Present	Same as in the INP-100 run	Absent	Present
INP-reduced-no-sedim	Present	Present	Same as in the INP-reduced run	Absent	Present

Table 1. Summary of simulations

56

Figure 1

1839

1840

1841

1842

1843

1844

1845

(a)

1846

1847 **Time (days)**

1848 **Figure 2a**

1849

1850

1851

1852

1853

1854

1855
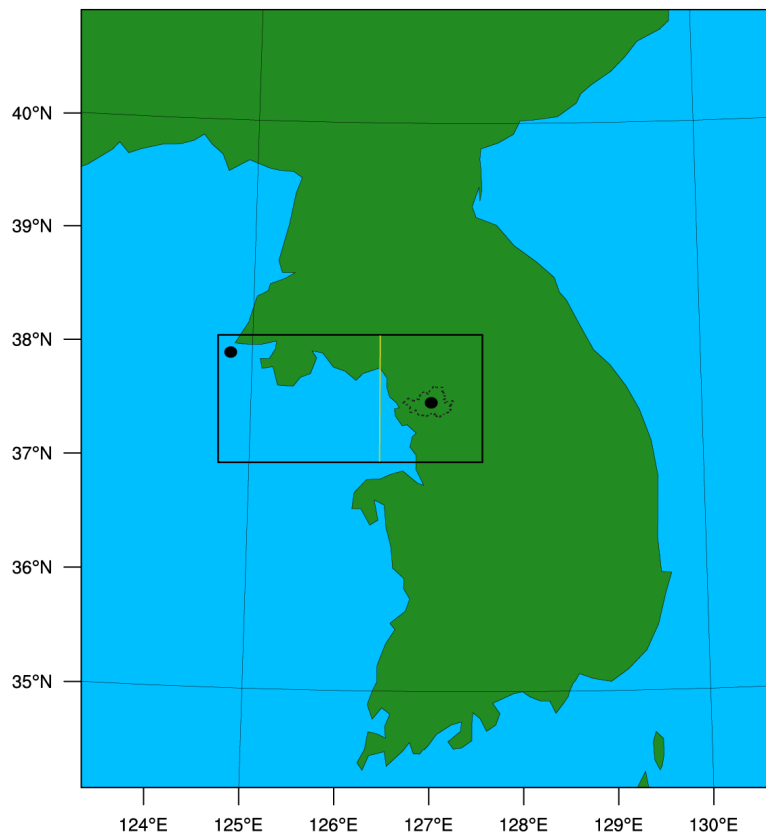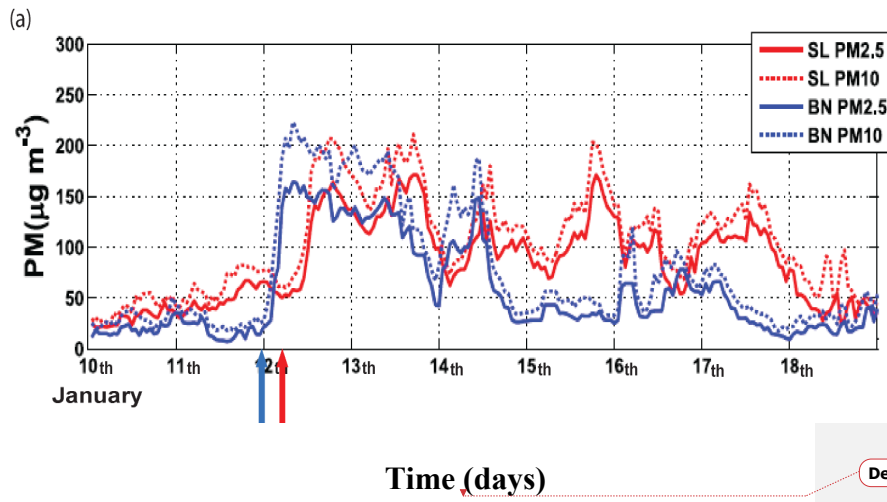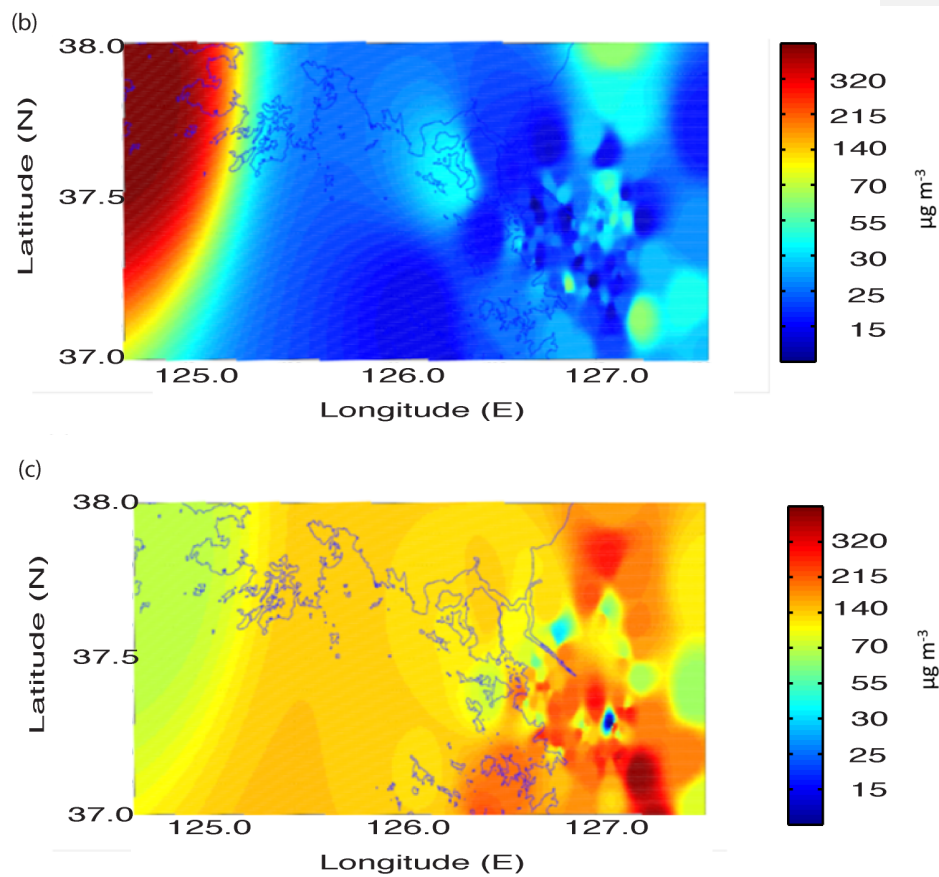
Figures 2b and 2c

 Figure 3

1867

1868

Figure 4

1869

1870

1871

1872

1873

1874

1875

1876

1877

1878

1879

1880

1881

1882

1883

1884

1885

1886

1887

1888
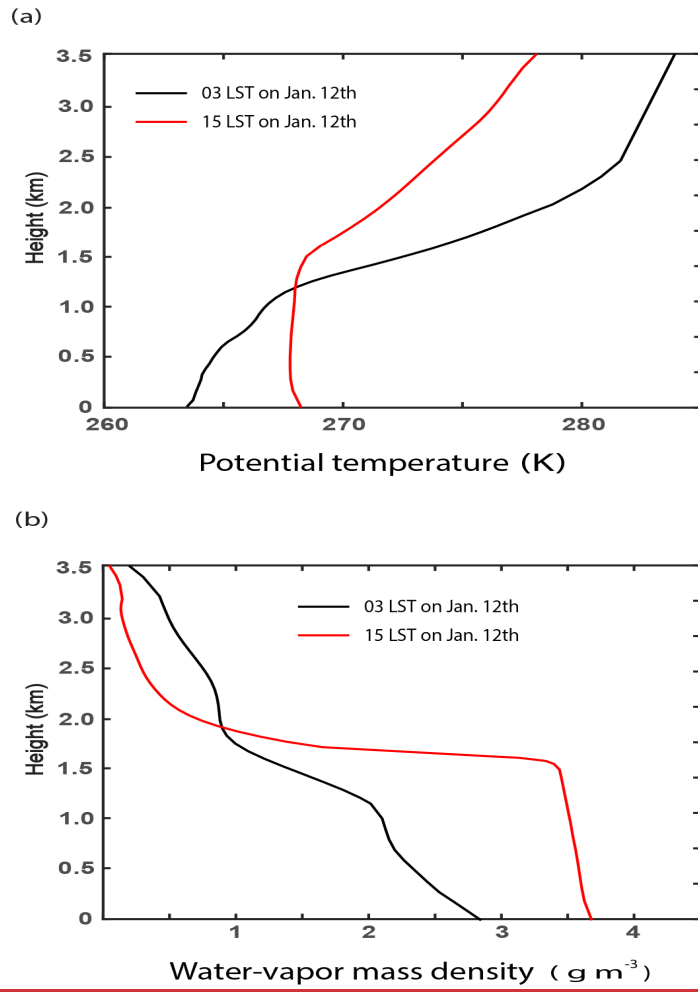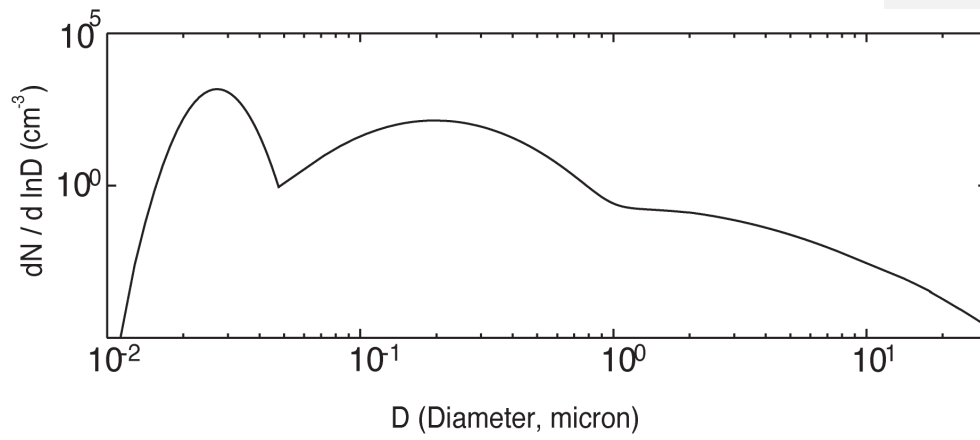
(a)
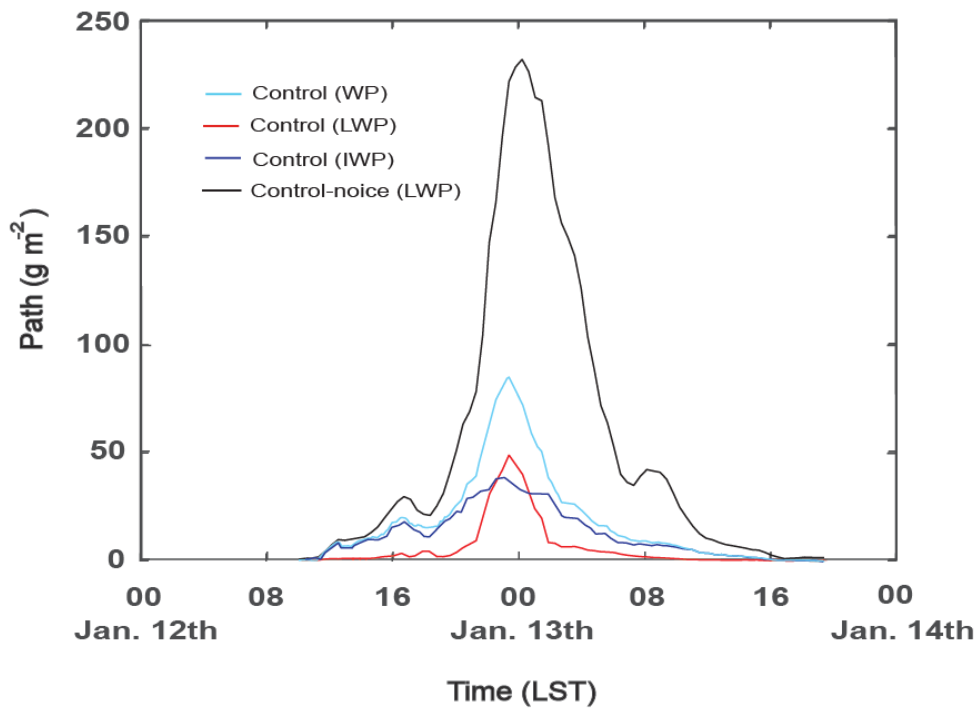
Figure 5a

Deleted: 3

1904
1905

1906
1907
1908
1909
1910
1911
1912
1913
1914
1915
1916
1917
1918

Figure 5b

1920

(c)

1921
1922
1923
1924

1925

1926

Figure 5c

(d)

1928

Figure 5d

1929

1930

1931

1932

1933

1934

(a)

1936

Figure 6a

1937

1938

1939

1940

1941

1942

1943

1944

1945

Figure 6b

1947

1948

1949

(a)

(b)
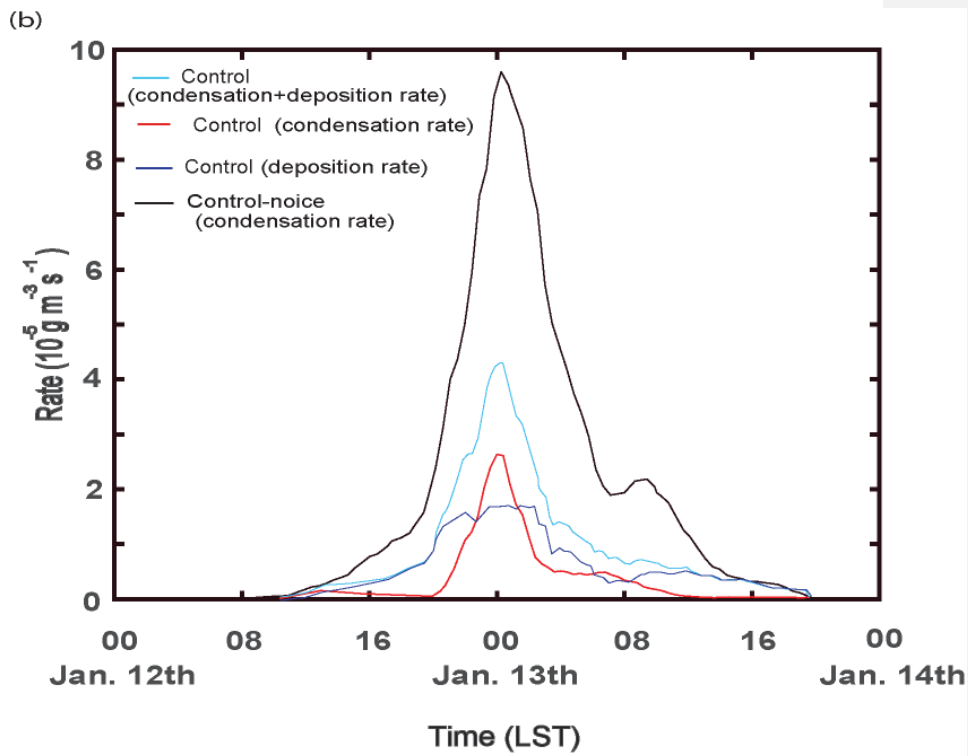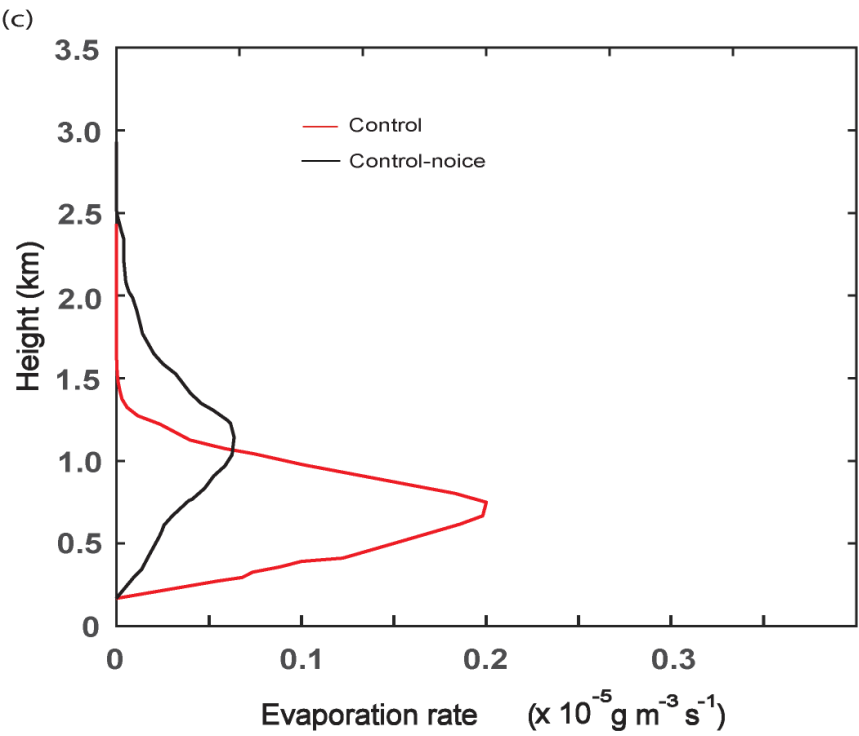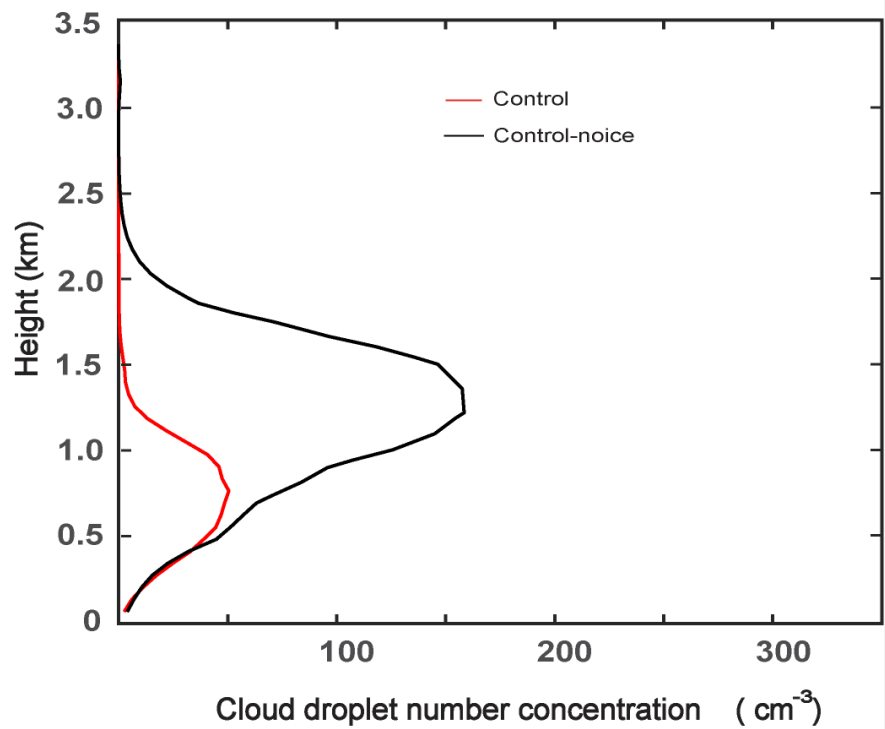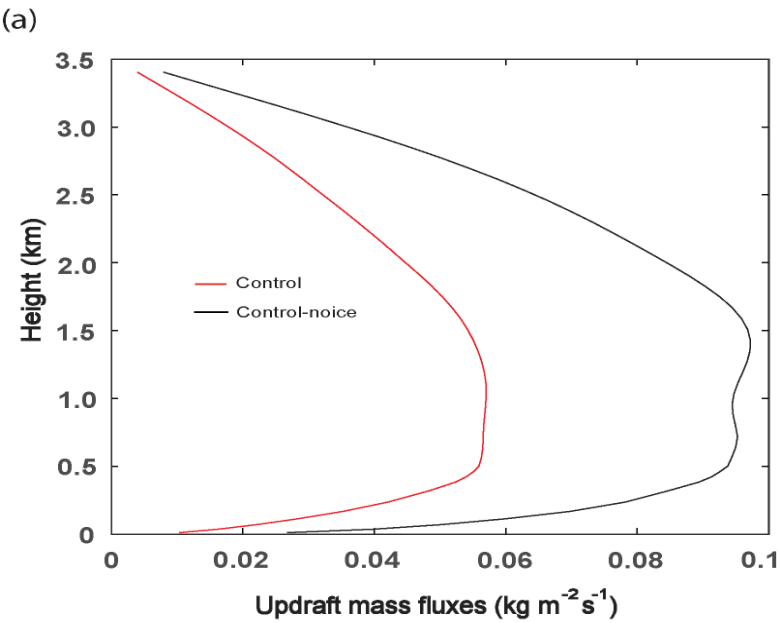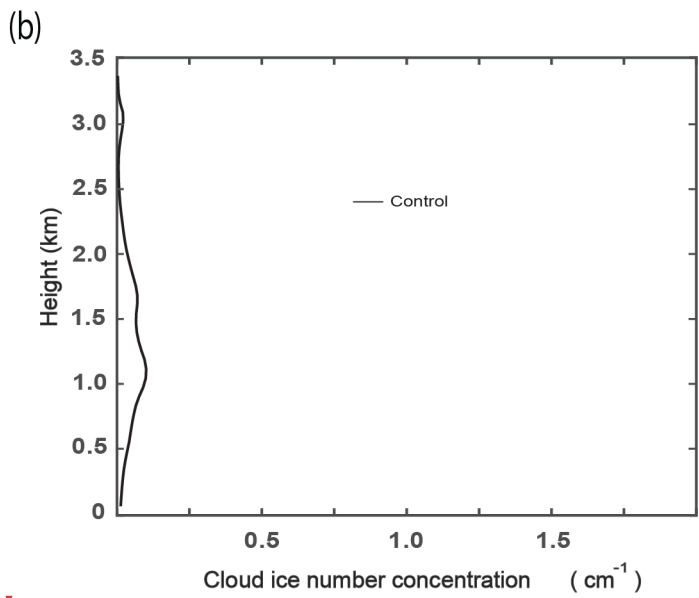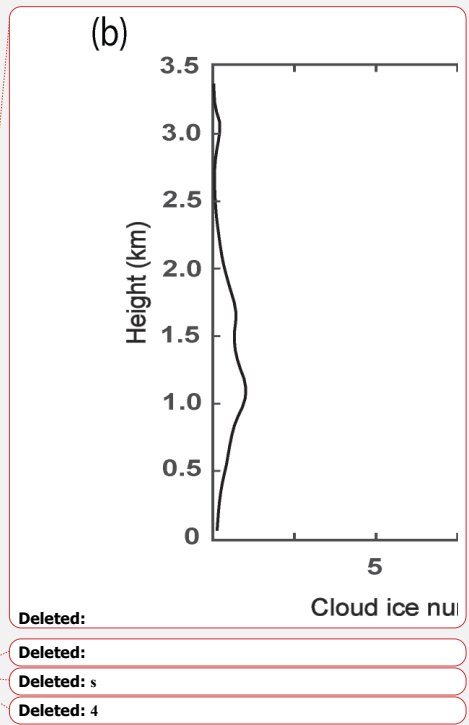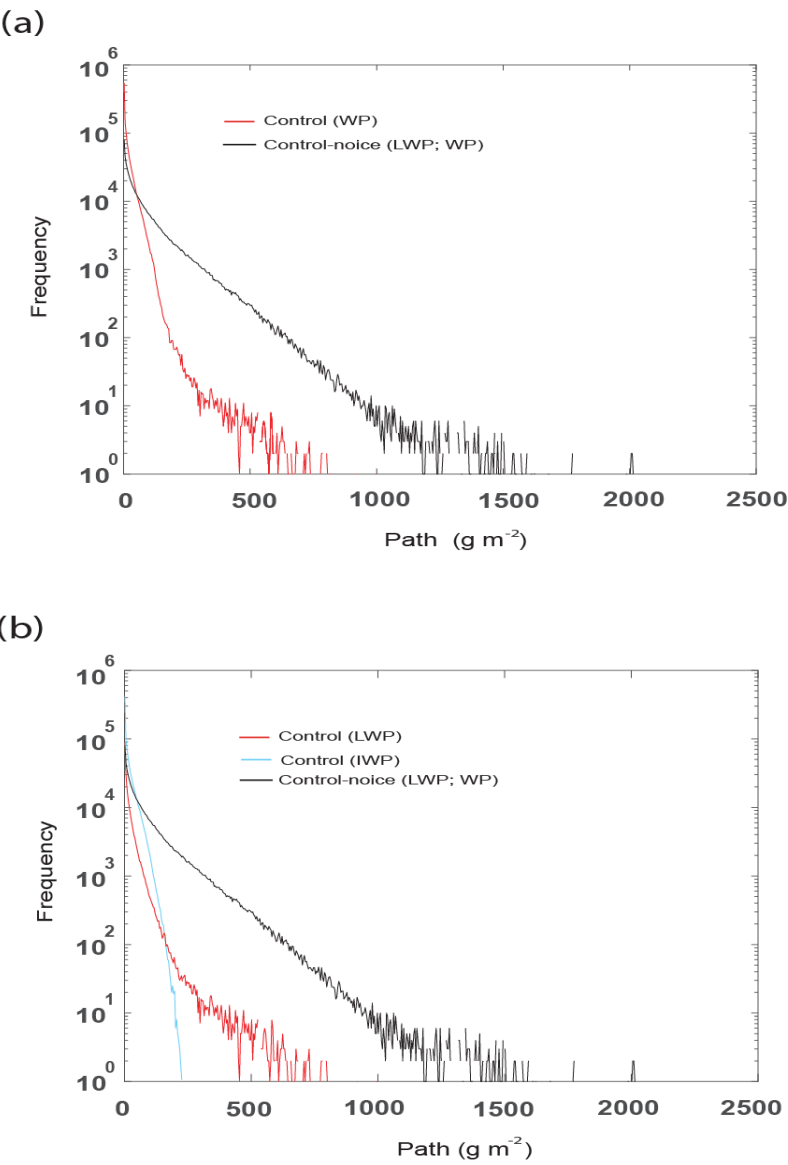
1954

1955   **Figures 7a and 7b**
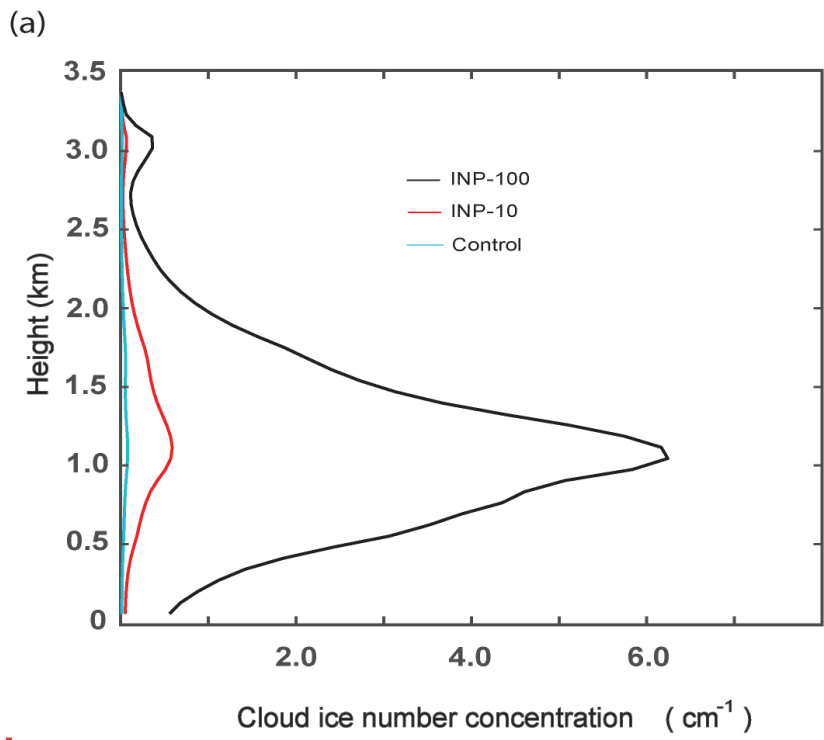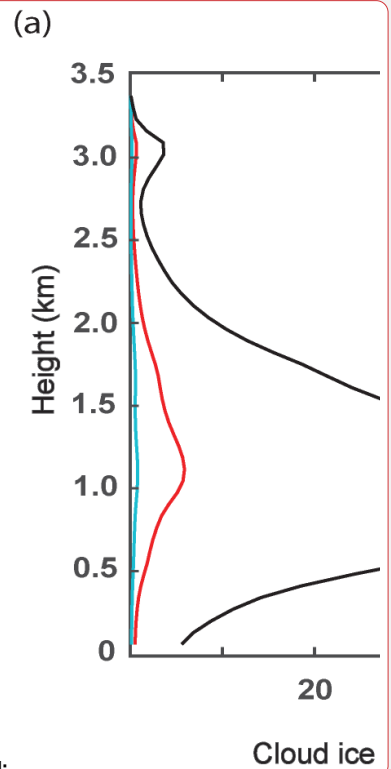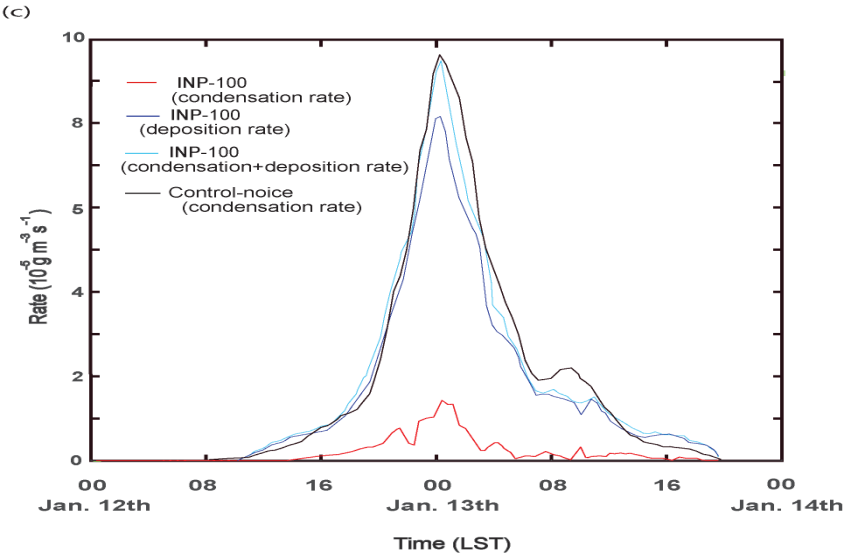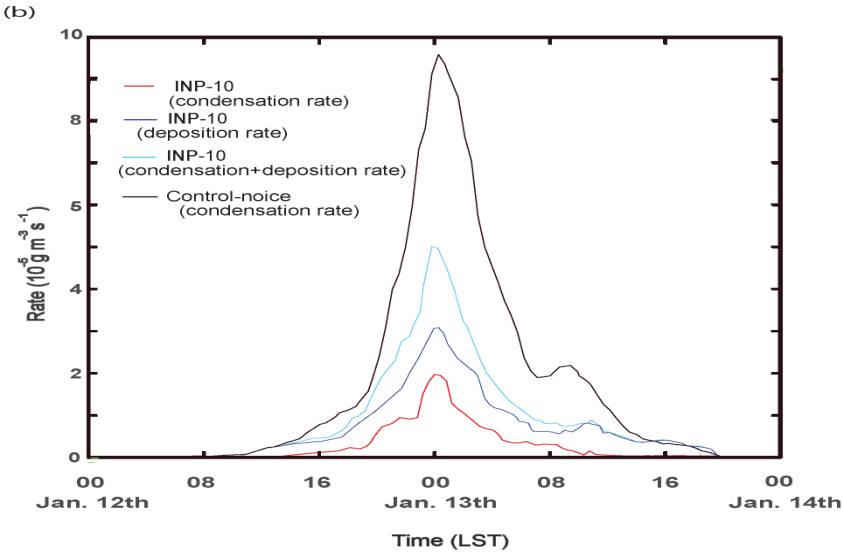
Figure 8a

 Figures 8b and 8c

Deleted:

Deleted: 6

Deleted: 6

(a)
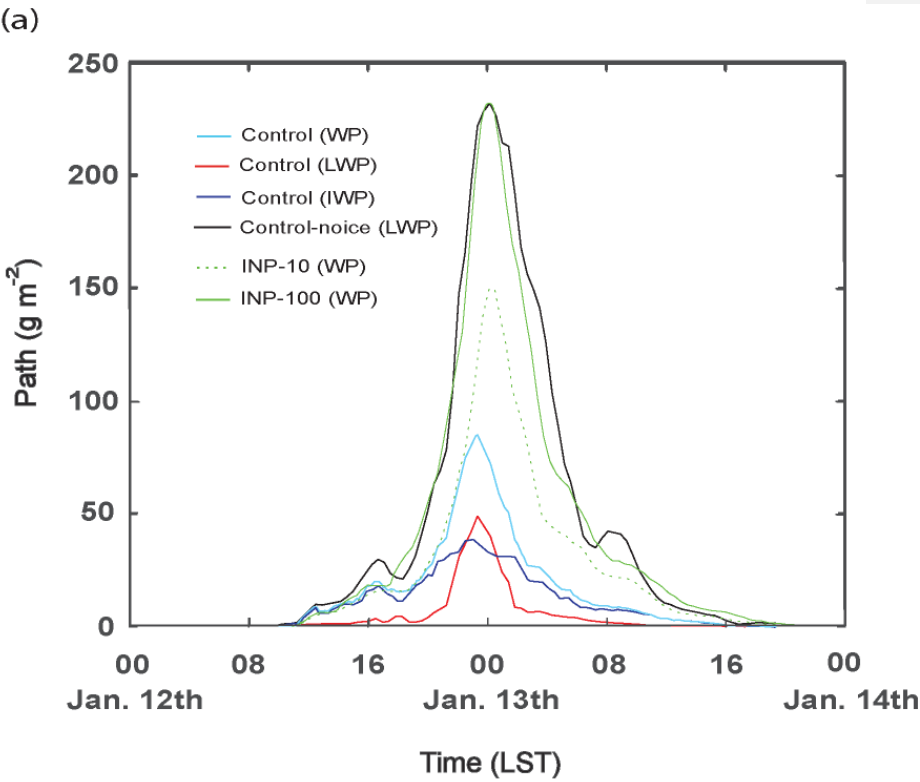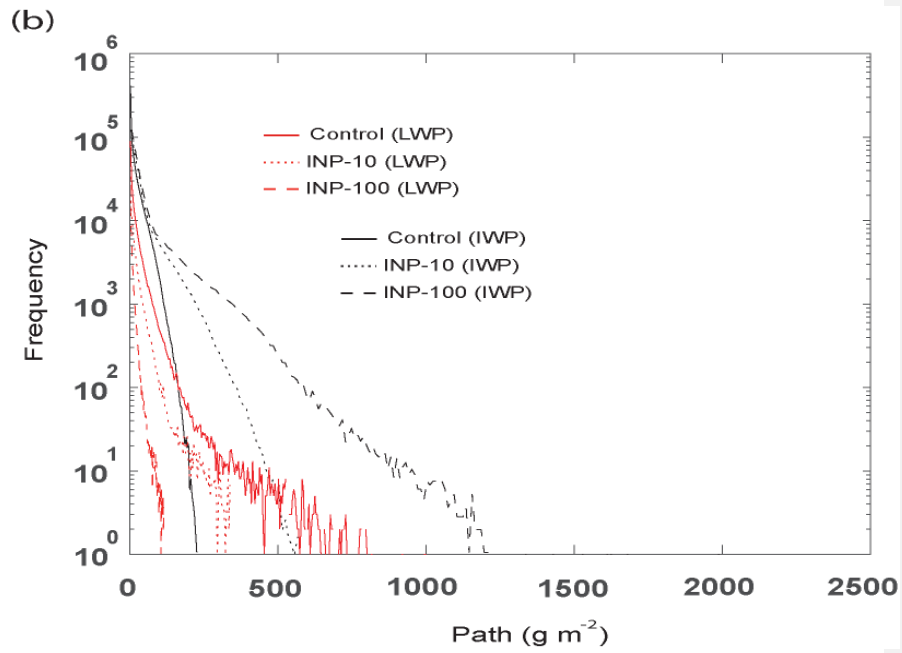
Figure 9a

Deleted: 7

Figure 9b

1979

1980

1981

1982

1983

1984

1985

1986

(a)
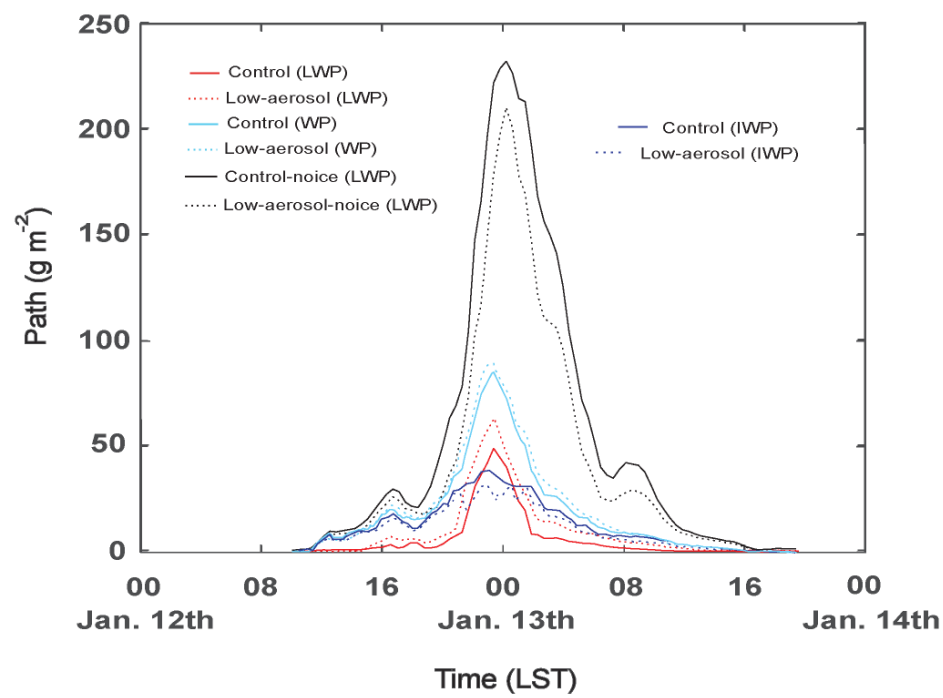
1988

1989   **Figure 10a**

1990

1991

1992

1993

1994

Deleted: 8

none

(b)

(c)

1996

1997
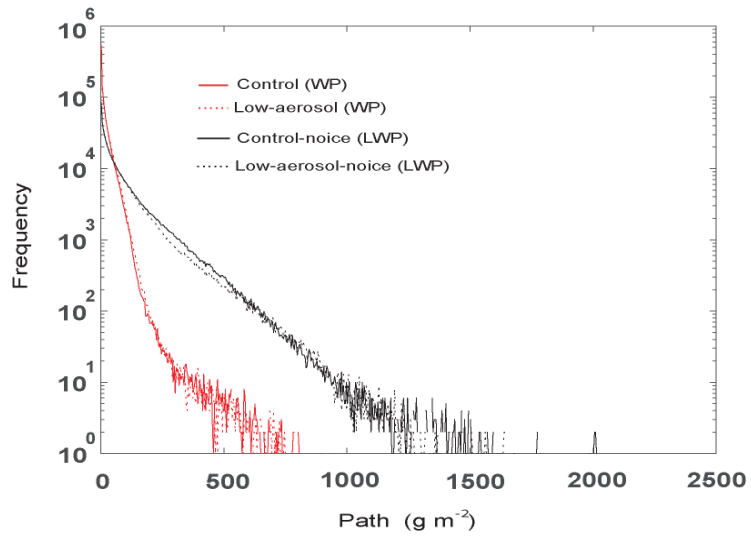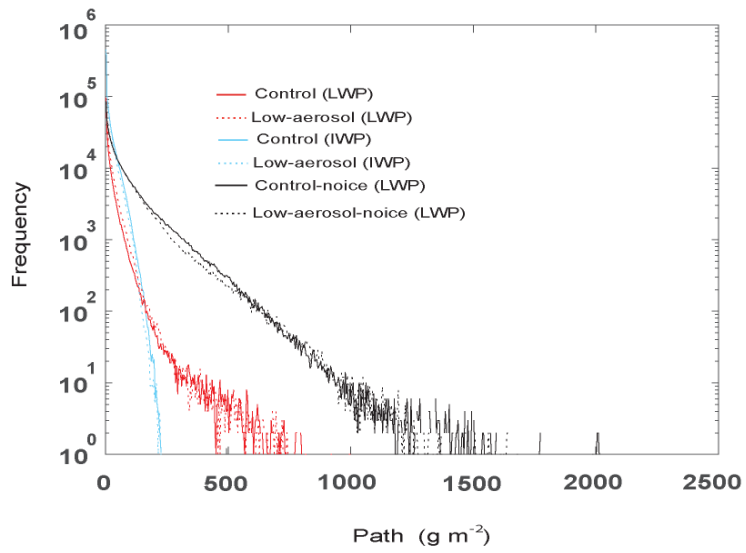
Figures 10b and 10c

Deleted: 8

Deleted: 8

Figure 11a

2000

2001

2002

2003

2004

2005

(b)
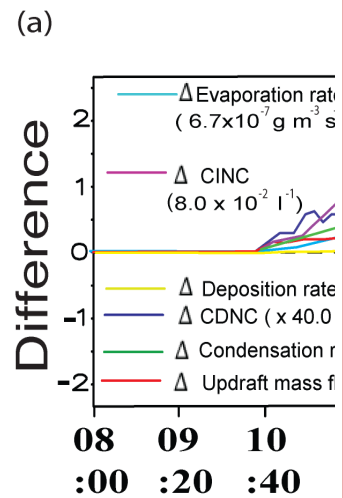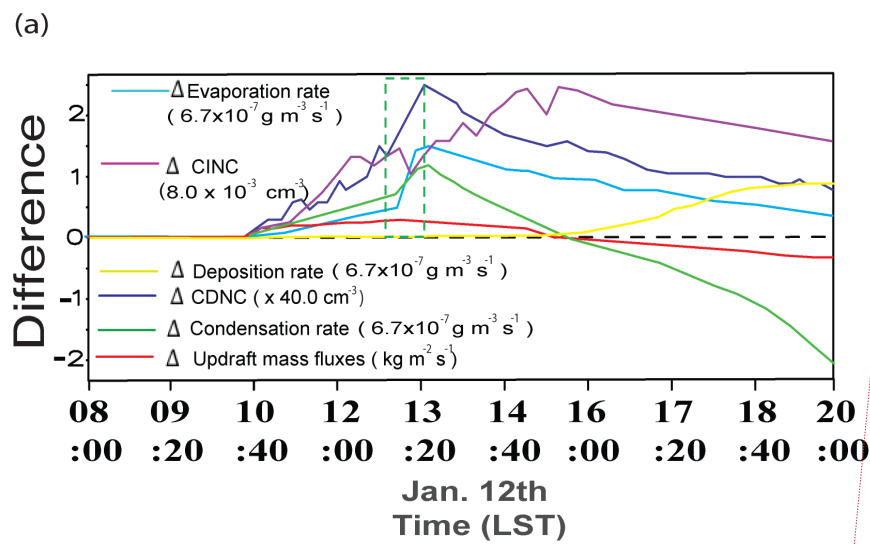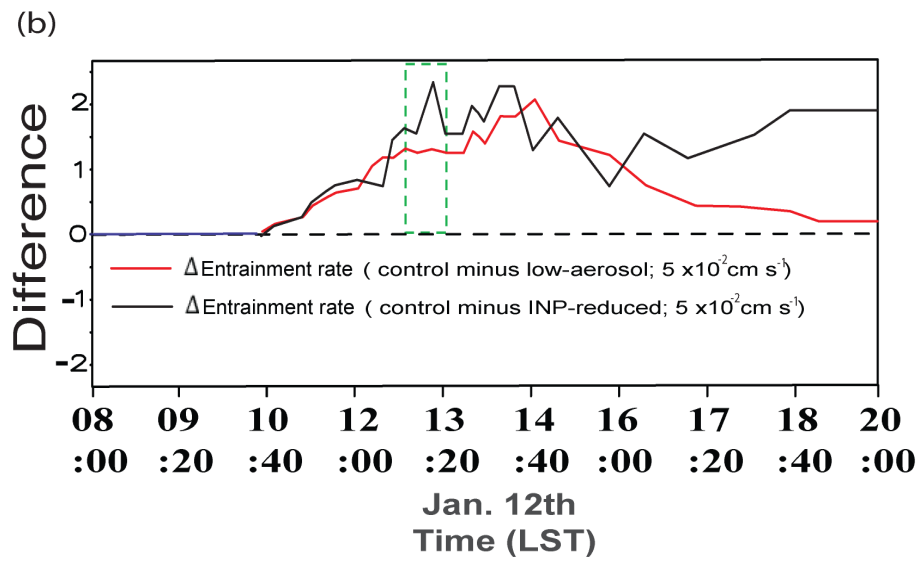
Figure 11b

2009

2010

2011

2012

2013

2014

2015

2016

2017

2019

(c)
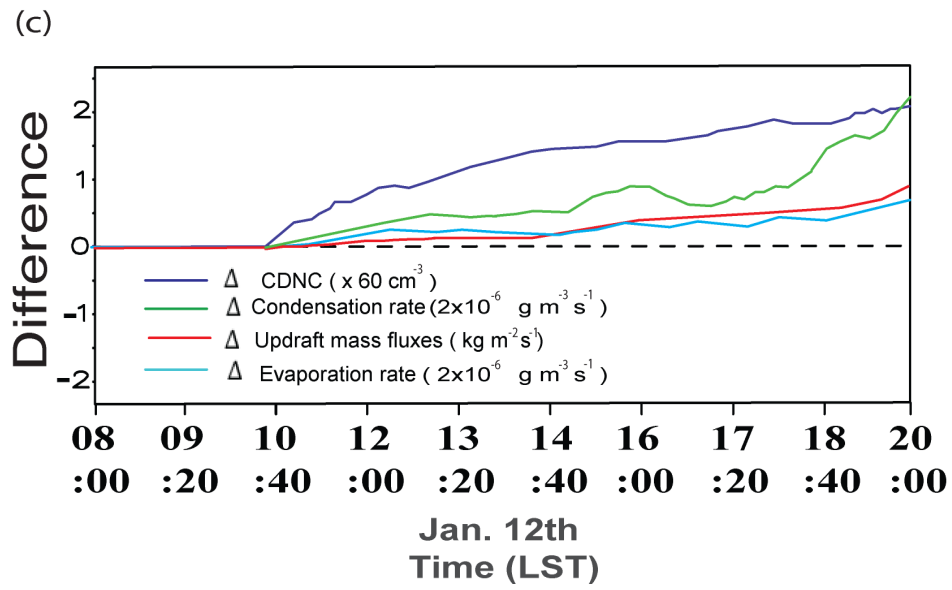
2020

2021 **Figure 11c**

2022

2023

2024

2025

2026

2027

2028

Figure 11d

2030

2031

2032

2033

2034

2035

2036

2037

(a)

(b)

2041

Figures 12a and 12b

2045

2046

2047

Figure 13

2049

Figure 14

2050

2051

2052